Dynamic sloshing in a rectangular vessel with porous baffles

M.R. Turner[1]

School of Mathematics and Physics, University of Surrey,
Guildford, Surrey GU2 7XH, UK

5th February 2024

The damping efficiency of vertical porous baffles is investigated for a dynamically coupled fluid-vessel system. The system comprises of a two-dimensional vessel, with a rectangular cross-section, partially filled with fluid, undergoing rectilinear motions with porous baffles obstructing the fluid motion. The baffles pierce the surface of the fluid, thus the problem can be considered as separate fluid filled regions of the vessel, connected by infinitely thin porous baffles, at which transmission conditions based on Darcy's law are applied. The fluid is assumed to be inviscid, incompressible and irrotational such that the flow in each region is governed by a velocity potential. The application of Darcy's law at the baffles is significant as it makes the system non-conservative, and thus the resulting characteristic equation for the normal modes leads to damped modes coupled to the moving vessel. Numerical evaluations of the characteristic equation show that the lowest frequency mode typically has the smallest decay rate, and hence will persist longest in an experimental setup. The maximum decay rate of the lowest frequency mode occurs when the baffles split the vessel into identically sized regions.

1   Introduction

When a vessel, partially filled with fluid, is constrained to move in some prescribed motion, the fluid within can experience complex motions. As the fluid sloshes back and forth in the vessel it interacts with the vessel walls, generating forces and moments on the vessel. If the vessel is free to move under the forces generated by the fluid motion (perhaps in some constrained manner) then this coupled motion could be stabilizing or destabilizing to the overall system. A simple everyday example of this instability is when we spill coffee while walking to our seat [1]. The destabilizing aspect of coupled sloshing can have disastrous effects, such as capsizing King crab boats [2], so being able to identify and mitigate against such effects is important. For example, the coffee spilling problem could be mitigated against using a 'carry cradle' which reduces the amplitude of the feedback response [3]. In the current paper we consider a simple model which mitigates against destabilization via the use of porous baffles.

---

[1]Corresponding Author: m.turner@surrey.ac.uk

Rigid impermeable baffles were first used to minimise sloshing in fuel tanks within the space industry [4, 5], mainly by simply blocking the fluid flow. They were also investigated for use in Tuned Liquid Dampers (TLDs), which are vessels partially filled with fluid, constrained to one-dimensional motions, with a spring acting as a restoring force of the system. Such dampers are typically used as stabilizers in highrise buildings to damp out oscillations induced by earthquakes or strong winds [6]. As well as just blocking the flow, baffles can also stabilize the system by altering the natural frequency of the system, such that forcing terms potentially act out of phase with the forcing frequency, causing flow velocities and accelerations to be less severe. Turner *et al.* [7] investigated such a scenario for multiple surface piercing impermeable baffles, which essentially split the vessel into multiple compartments. They found the frequency of the modes in the system were altered by the baffles and that potential internal resonances existed. Alemi Ardakani & Turner [8] devised an effective and efficient numerical scheme to model this system in the limit of shallow-water fluids, and investigated the effect on the system when considering a nonlinear spring.

Porous baffles have been well studied in the context of TLDs and ship fuel tanks, for example, because in these cases the baffles provide an important damping mechanism to the fluid in the system [9, 10]. Even the simplest scenario of forced sloshing in a rectangular vessel has been well studied via experimental and numerical simulations, using submerged or surface piercing baffles, set in various configurations such as vertical, horizontal or slanted baffles [11, 12, 13, 14, 15, 16, 17, 18, 19, 20]. Whilst there are a varying array of results on such systems, the key messages are that the width of the baffles are not hugely significant, but the position and composition of the baffles are key to the amount of damping observed in the system [21, 22]. The construction of the porous baffle (e.g. randomly drilled porous metal blocks or regular perforated plates etc.) also has a significant effect on how best to model the transmission of the fluid through the baffle. Differing approaches to modelling the transmission conditions [23] include using Darcy's law [24, 25, 26, 27] or using a pressure drop condition [28, 29], which has also been applied to other water wave problems [30, 31].

The originality of the current paper is, we examine the effect of porous, surface piercing, baffles in a dynamically coupled rectangular TLD system with a linear restoring force. The novel difference here compared to the forced problems considered above, is that the motion of the vessel, which we assume is able to move in a single space dimension, is not known a priori and needs to be solved for. In order to gain a physical understanding of the significance of the baffle, we consider an idealised system consisting of an inviscid, incompressible, irrotational fluid in a rectangular vessel, where the vessel motion is modelled by a forced pendulum equation. Such an approximation is suitable over relatively short time periods, where viscosity doesn't have time to act significantly. The current formulation could be amended to incorporate viscosity by including artificial dissipation [32, 33] or by adding additional terms to the free-surface boundary conditions [34]. The fluid transmission across the baffle is modelled using Darcy's law, such that the velocity of the fluid at the baffle is directly proportional to the pressure difference across the baffle itself. Unlike for the zero baffle and impermeable baffle dynamical problems considered previously [35, 7], the porous baffle makes the system nonconservative and hence energy is extracted from the system. The main goal of this paper is to show that for a single baffle system an analytic characteristic equation can be derived for the natural frequencies of the system, to identify the parameters for which the system decays the fastest and to quantify how this maximum decay rate varies in terms of these parameters.

The current paper is laid out as follows. In §2 we formulate the governing nonlinear equations, and seek normal mode solutions after linearising about a quiescent state. For the single baffle problem an explicit analytical characteristic equation is derived, which is solved numerically. Results of the characteristic equation for a single baffle are presented in §3.1 including both complex frequency values, and free-surface elevations, while multiple baffle cases are considered in §3.2. Concluding remarks are given in §4.

2   Formulation

We consider the two-dimensional coupled sloshing system as detailed in figure 1. Here (X, Y) is a fixed coordinate system, while (x, y) are Cartesian coordinates fixed to the moving vessel. The coordinate systems are related via,

$$X = x + q(t), \qquad Y = y + y_0,$$

where $q(t)$ is the time dependent extension of the spring attached to the vessel and the wall at $X = 0$, and y_0 is a constant.
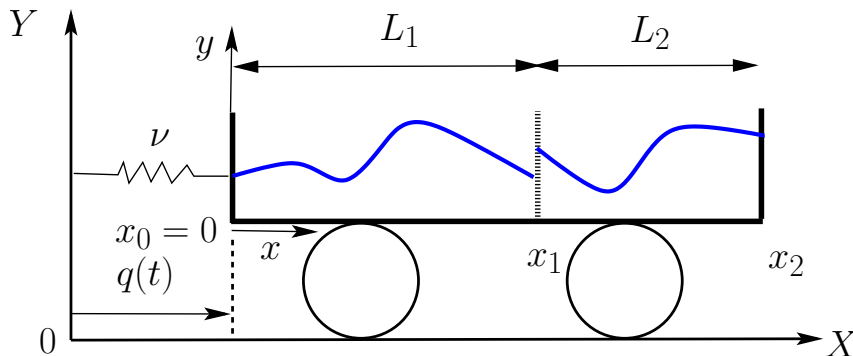

Figure 1: Schematic diagram of a two-dimensional fluid-filled vessel with rectangular cross-section, and a porous baffle at $x = x_1$. The vessel is restricted to move in x-direction and is connected to $X = 0$ via a linear spring of stiffness ν. The function $q(t)$ denotes the extension of the spring from its equilibrium position.

We derive the system of equations for a single baffle for simplicity, but the approach can be extended to incorporate any number of baffles. We consider the vessel divided into two regions by a porous baffle at $x = x_1$, labeled region 1 and region 2 from left to right, with $x \in [0, x_1]$ for region 1 and $x \in [x_1, x_2]$ in region 2. The lengths of each region are L_1 and L_2 respectively, hence $x_1 = L_1$ and $x_2 = L_1 + L_2$, and the fluid occupies the region

$$x_{j-1} \le x \le x_j \quad \text{and} \quad 0 \le y \le h_j(x, t),$$

for $j = 1, 2$, with $x_0 = 0$. Our ultimate goal in this work is to linearise about a quiescent state, hence the fluid velocities in the system are assumed to be low enough such that the fluid can be modelled as inviscid, incompressible and irrotational, without any wave breaking episodes. In this scenario the velocity components relative to the moving frame in each region $(\widehat{u}_j, \widehat{v}_j)$ can be derived in terms of a velocity potential $\phi_j(x, y)$ such that

$$\widehat{u}_j = \frac{\partial \phi_j}{\partial x} - \dot{q}(t), \quad \widehat{v}_j = \frac{\partial \phi_j}{\partial y}. \tag{2.1}$$

3

Mass continuity then states that the velocity potentials satisfy Laplace's equation

$$\frac{\partial^2 \phi_j}{\partial x^2} + \frac{\partial^2 \phi_j}{\partial y^2} = 0, \tag{2.2}$$

in each region.

The fluid pressure in each region is found via the unsteady Bernoulli equation which states

$$\frac{p_j}{\rho} + \frac{\partial \phi_j}{\partial t} + \frac{1}{2}\left[\left(\frac{\partial \phi_j}{\partial x}\right)^2 + \left(\frac{\partial \phi_j}{\partial y}\right)^2\right] - \dot{q}\frac{\partial \phi_j}{\partial x} + gy + \frac{1}{2}\dot{q}^2 = 0,$$

where ρ is the constant density of the fluid, the dot indicates differentiation with respect to t and the Bernoulli constant has been absorbed into a linear time-dependent term of ϕ_j. Evaluating this on the free-surface ($y = h_j(x,t)$) gives the dynamic boundary condition ($p_j = 0$) as

$$\frac{\partial \phi_j}{\partial t} + \frac{1}{2}\left[\left(\frac{\partial \phi_j}{\partial x}\right)^2 + \left(\frac{\partial \phi_j}{\partial y}\right)^2\right] - \dot{q}\frac{\partial \phi_j}{\partial x} + gh_j + \frac{1}{2}\dot{q}^2 = 0, \tag{2.3}$$

while the corresponding kinematic boundary condition is

$$\frac{\partial h_j}{\partial t} + \left(\frac{\partial \phi_j}{\partial x} - \dot{q}\right)\frac{\partial h_j}{\partial x} = \frac{\partial \phi_j}{\partial y}, \tag{2.4}$$

for $j = 1, 2$. Zero penetration boundary conditions are applied on the bottom and side walls of the vessel, thus

$$\left.\frac{\partial \phi_j}{\partial y}\right|_{y=0} = 0, \quad \text{and} \quad \left.\frac{\partial \phi_1}{\partial x}\right|_{x=0} = \left.\frac{\partial \phi_2}{\partial x}\right|_{x=x_2} = \dot{q}, \tag{2.5}$$

in the moving frame. We assume that the effects of the front and back walls of the vessel are negligible, such that our two-dimensional assumption is valid. Such an assumption has been proved to be valid such as in the work of [36] who showed the two-dimensional approximation agreed very well with experimental results.

The baffle at $x = x_1$ is porous and as such, fluid is able to transmit between the regions. We do not physically model the fluid flow through the baffle, and instead use a transition condition to link the fluid velocities in the bulk fluid at the baffle to the pressure drop across the baffle. In this paper our main goal is to consider linear solutions to the governing equations in §2.1 about a fluid at rest. Hence our interest is in small magnitude fluid motions. Given this assumption, and the fact that the baffle is coherent, we apply a transmission condition based upon Darcy's law [24, 37], namely that the velocity is continuous across the baffle with

$$\left.\frac{\partial \phi_1}{\partial x}\right|_{x=x_1} = \left.\frac{\partial \phi_2}{\partial x}\right|_{x=x_1} = \dot{q} - \frac{\beta}{\rho}\left(p_2(x_1, y, t) - p_1(x_1, y, t)\right). \tag{2.6}$$

At larger fluid velocities where nonlinear effects are more important the transmission condition can modelled via a Darcy-Forchheimer model [38] which includes a quadratic velocity term. At very large velocities this quadratic term dominates the transmission condition and a model as in [29] becomes applicable to leading order.

In (2.6) β is a complex coefficient which describes the porosity of the baffle, and has the dimensions of sm^{-1}. The complex form of $\beta = \beta_r + i\beta_i$ ($\beta_r, \beta_i > 0$) is such that the

real part represents the resistance effect of the baffle against the flow, while the imaginary part represents the inertial effect of the fluid in the baffle [25, 27, 39, 40]. Experimental results for perforated plates show that $\beta_i \approx 0.1\beta_r$ [41] and hence is typically small, so we will mostly consider $\beta_i = 0$, but we do consider cases with $\beta_i \neq 0$ to show the effect of this quantity. The case $|\beta| = 0$ indicates that the baffle is impermeable (as considered in [7]), while $|\beta| \to \infty$ indicates the baffle has no effect on the fluid motion, hence its presence can be neglected, and the vessel reduces to a single region vessel (as considered in [35]). In this work we consider our porosity parameter β to be a constant and we do not consider how its value relates to the physical construction of the baffle. In more complex scenarios such as in [29], the transmission rate of the baffle can be related to more physical parameters such as the solidity ratio. However, as we are not quantitatively fitting our results to experiments we do not go to this extent here.

The equation for the vessel motion, which couples to the fluid motion, is given via the forced linear pendulum equation

$$m_v \ddot{q} + \nu q = -\frac{\mathrm{d}}{\mathrm{d}t} \left[\int_0^{L_1} \int_0^{h_1} \rho \frac{\partial \phi_1}{\partial x} \, \mathrm{d}y \mathrm{d}x + \int_{L_1}^{L_1+L_2} \int_0^{h_2} \rho \frac{\partial \phi_2}{\partial x} \, \mathrm{d}y \mathrm{d}x \right], \qquad (2.7)$$

where ν is the linear stiffness of the spring connected to the vessel. Here we assume a linear spring only, for simplicity, as we will be seeking modal solutions in §2.2.

Equations (2.2)-(2.7) denote the nonlinear system of equations which govern the coupled sloshing problem for the fluid and vessel motions.

2.1   Linearised Equations

We wish to determine the modal solutions of the linearised system about a quiescent state. These would be the natural frequencies that the system would want to oscillate at if initialized appropriately. In a quiescent state we assume the fluid has equilibrated such that $h_1 = h_2 = H$, and that the pressure in each region is hydrostatic $p_j = \rho g(H - y)$. Therefore we introduce the perturbed quantities, denoted with a bar, such that

$$
\begin{aligned}
q(t) &= \epsilon \overline{q}(t), \\
h_j(x,t) &= H + \epsilon \overline{h}_j(x,t), \\
\phi_j(x,y,t) &= \epsilon \overline{\phi}_j(x,y,t), \\
p_j(x,y,t) &= \rho g(H - y) + \epsilon \overline{p}_j(x,y,t),
\end{aligned}
$$

where $0 < \epsilon \ll 1$ indicates the size of the perturbation and is small enough for linearisation. Substituting these expressions into (2.2)-(2.7) and retaining terms of $O(\epsilon)$ only, leads to the following set of linear equations

$$\overline{\phi}_{jxx} + \overline{\phi}_{jyy} = 0, \quad 0 < y < H, \quad x_{j-1} < x < x_j, \qquad (2.8)$$

$$\overline{\phi}_{jy}(x,0,t) = 0, \qquad (2.9)$$

$$\overline{\phi}_{1x}(0,y,t) = \overline{\phi}_{2x}(x_2,y,t) = \dot{\overline{q}}, \qquad (2.10)$$

$$\overline{\phi}_{1x}(x_1,y,t) = \overline{\phi}_{2x}(x_1,y,t) = \dot{\overline{q}} - \frac{\beta}{\rho}(\overline{p}_2(x_1,y,t) - \overline{p}_1(x_1,y,t)), \qquad (2.11)$$

$$\overline{\phi}_{jt} + g\overline{h}_j = 0 \quad \text{on} \quad y = H, \qquad (2.12)$$

$$\overline{h}_{jt} = \overline{\phi}_{jy} \quad \text{on} \quad y = H, \qquad (2.13)$$

5

with the pressure perturbation given by

$$\frac{\overline{p}_j}{\rho} + \overline{\phi}_{jt} = 0, \tag{2.14}$$

and the vessel equation becoming

$$m_v\ddot{\overline{q}} + \nu\overline{q} = -\frac{\mathrm{d}}{\mathrm{d}t}\left[\int_0^{L_1}\int_0^H \rho\frac{\partial\overline{\phi}_1}{\partial x}\,\mathrm{d}y\mathrm{d}x + \int_{L_1}^{L_1+L_2}\int_0^H \rho\frac{\partial\overline{\phi}_2}{\partial x}\,\mathrm{d}y\mathrm{d}x\right]. \tag{2.15}$$

Here, and in the remainder of the paper, the subscripts x, y, t denote partial derivatives.

The governing set of linear equations can be manipulated into a problem dependent solely on the velocity potential $\overline{\phi}_j$ and the spring extension $\overline{q}$ by combining the free-surface conditions (2.12) and (2.13) to eliminate $\overline{h}_j$

$$\overline{\phi}_{jtt} + g\overline{\phi}_{jy} = 0 \quad \text{on} \quad y = H, \tag{2.16}$$

and by using the pressure perturbation (2.14) to write the boundary conditions on the porous baffle as

$$\overline{\phi}_{1x}(x_1, y, t) = \overline{\phi}_{2x}(x_1, y, t) = \dot{\overline{q}} + \beta\left[\overline{\phi}_{2t}(x_1, y, t) - \overline{\phi}_{1t}(x_1, y, t)\right]. \tag{2.17}$$

The resulting linear equations can be solved by seeking normal mode solutions.

2.2   Normal Modes

We seek modal solutions of the linear system of equations (2.8)-(2.10) and (2.15)-(2.17) so as to identify the natural frequencies of the system, which in a physical system, comprise the components of all solutions via superposition. To identify the modal solutions we write

$$\overline{\phi}_j(x, y, t) = \widehat{\phi}_j(x, y)e^{\mathrm{i}\omega t}, \qquad \overline{q}(t) = \widehat{q}e^{\mathrm{i}\omega t}. \tag{2.18}$$

Unlike for the impermeable baffle problem considered in [7], the form of the solution in (2.18) consists of a superposition of both $\sin\omega t$ and $\cos\omega t$ terms, and also allows for the consideration of ω being complex.

Substituting (2.18) into the governing linear equations leads to the following boundary value problem for the hatted variables

$$\widehat{\phi}_{jxx} + \widehat{\phi}_{jyy} = 0, \quad 0 < y < H, \quad x_{j-1} < x < x_j, \tag{2.19}$$

$$\widehat{\phi}_{jy}(x, 0) = 0, \tag{2.20}$$

$$\widehat{\phi}_{1x}(0, y) = \widehat{\phi}_{2x}(x_2, y) = \mathrm{i}\omega\widehat{q}, \tag{2.21}$$

$$\widehat{\phi}_{1x}(x_1, y) = \widehat{\phi}_{2x}(x_1, y) = \mathrm{i}\omega\widehat{q} + \mathrm{i}\beta\omega\left(\widehat{\phi}_2(x_1, y) - \widehat{\phi}_1(x_1, y)\right), \tag{2.22}$$

$$\omega^2\widehat{\phi}_j(x, H) = g\widehat{\phi}_{jy}(x, H), \tag{2.23}$$

with vessel equation

$$\left[\nu - m_v\omega^2\right]\widehat{q} = \mathrm{i}\omega\left[\int_0^{L_1}\int_0^H \rho\frac{\partial\widehat{\phi}_1}{\partial x}\,\mathrm{d}y\mathrm{d}x + \int_{L_1}^{L_1+L_2}\int_0^H \rho\frac{\partial\widehat{\phi}_2}{\partial x}\,\mathrm{d}y\mathrm{d}x\right]. \tag{2.24}$$

The homogeneous nature of the free-surface and bottom boundary conditions means the problem lends itself to seeking a solution for $\widehat{\phi}_j$ in each region as a superposition

6

of vertical eigenmodes. Properties of these vertical eigenmodes have been explored in [42], and for the coupled, single region, sloshing problem in [35]. Hence we quote here the relevant results for this paper, and refer the reader to these works for full details. Therefore the separable solution to (2.19) which satisfies (2.20) and (2.23) can be written as

$$\widehat{\phi}_j(x, y) = \sum_{n=0}^{\infty} A_{jn}(x)\psi_n(y),\qquad(2.25)$$

where the vertical eigenmodes $\psi_n(y)$ have the form

$$\psi_0(y) = \frac{1}{N_0}\cosh k_0 y, \quad \text{and} \quad \psi_n(y) = \frac{1}{N_n}\cos k_n y \quad \text{for} \quad n \geq 1.$$

The constants N_0 and N_n are normalization constants given by

$$N_0 = \sqrt{\frac{1}{2}\left(1 + \frac{\sinh 2k_0 H}{2k_0 H}\right)}, \qquad N_n = \sqrt{\frac{1}{2}\left(1 + \frac{\sin 2k_n H}{2k_n H}\right)},$$

while the eigenvalues k_0 and k_n satisfy

$$k_0 H \tanh k_0 H - \frac{\omega^2 H}{g} = 0,\qquad(2.26)$$

$$k_n H \tan k_n H + \frac{\omega^2 H}{g} = 0 \quad \text{for} \quad n \geq 1,\qquad(2.27)$$

which derive from the characteristic equation

$$\frac{\omega^2 H}{g}\cos\left(H\sqrt{\lambda}\right) + \left(H\sqrt{\lambda}\right)\sin\left(H\sqrt{\lambda}\right) = 0,$$

where λ is the eigenvalue.

In [42] and [35], where these eigenmodes are discussed, the frequency ω is real. Hence the first eigenvalue of the system is negative, $\lambda_0 = -k_0^2$ ($\sqrt{\lambda_0}$ being purely imaginary), and is associated with the 'wave mode', while the rest are positive, $\lambda_n = k_n^2$ $n \geq 1$, and are associated with the 'evanescent modes'. In the case when ω is complex, all the eigenvalues λ_n move off the real axis and become complex, and hence it may seem that the distinction between the wave mode and the evanescent modes becomes less obvious. However, in this case there is a single mode with $\text{Re}(\lambda_0 = -k_0^2) < 0$, while the other modes have $\text{Re}(\lambda_n = k_n^2) > 0$ and so we still find a wave mode plus evanescent modes structure even when ω is complex. Hence we still use these terms when describing the modes of the system.

The forms of the functions $A_{jn}(x)$ are found by satisfying Laplace's equation, which after satisfying the rigid wall boundary conditions (2.21) in the respective region, can be written as

$$A_{10}(x) = B_{10}\cos k_0 x + \frac{i\omega\widehat{q}c_0}{k_0}\sin k_0 x,\qquad(2.28)$$

$$A_{1n}(x) = B_{1n}\cosh k_n x + \frac{i\omega\widehat{q}c_n}{k_n}\sinh k_n x \quad \text{for} \quad n \geq 1,\qquad(2.29)$$

$$A_{20}(x) = B_{20}\cos k_0(x - x_2) + \frac{i\omega\widehat{q}c_0}{k_0}\sin k_0(x - x_2),\qquad(2.30)$$

$$A_{2n}(x) = B_{2n}\cosh k_n(x - x_2) + \frac{i\omega\widehat{q}c_n}{k_n}\sinh k_n(x - x_2) \quad \text{for} \quad n \geq 1,\qquad(2.31)$$

7

where B_{jn} for $j = 1, 2$ and $n \geq 0$ are constants to be determined. The constants c_0 and c_n come from expanding the unit function in terms of the vertical eigenfunctions, and are given by

$$c_0 = \frac{1}{N_0} \frac{\sinh k_0 H}{k_0 H}, \qquad c_n = \frac{1}{N_n} \frac{\sin k_n H}{k_n H}. \tag{2.32}$$

Satisfying the conditions (2.22) at the porous baffle $x = x_1 = L_1$ reduces to the 4 equations

$$k_0 \sin k_0 L_1 B_{10} + k_0 \sin k_0 L_2 B_{20} = -i\omega c_0 (\cos k_0 L_2 - \cos k_0 L_1)\widehat{q}, \tag{2.33}$$

$$(k_0 \sin k_0 L_1 - i\omega\beta \cos k_0 L_1) B_{10} + i\beta\omega \cos k_0 L_2 B_{20}$$
$$= \omega c_0 \left[i(\cos k_0 L_1 - 1) - \frac{\beta\omega}{k_0}(\sin k_0 L_1 + \sin k_0 L_2) \right] \widehat{q}, \tag{2.34}$$

$$k_n \sinh k_n L_1 B_{1n} + k_n \sinh k_n L_2 B_{2n} = i\omega c_n (\cosh k_n L_2 - \cosh k_n L_1)\widehat{q}, \tag{2.35}$$

$$(k_n \sinh k_n L_1 + i\omega\beta \cosh k_n L_1) B_{1n} - i\beta\omega \cosh k_n L_2 B_{2n}$$
$$= \omega c_n \left[i(1 - \cosh k_n L_1) + \frac{\beta\omega}{k_n}(\sinh k_n L_1 + \sinh k_n L_2) \right] \widehat{q}, \tag{2.36}$$

for $n \geq 1$. The second pair of equations (2.35) and (2.36) for $\mathbf{b} = (B_{1n}, B_{2n})^T$ can be written in matrix form $\mathbf{A}\mathbf{b} = \mathbf{q}$, where

$$\mathbf{q} = \omega c_n \left[\begin{array}{c} i(\cosh k_n L_2 - \cosh k_n L_1) \\ i(1 - \cosh k_n L_1) + \frac{\beta\omega}{k_n}(\sinh k_n L_1 + \sinh k_n L_2) \end{array} \right] \widehat{q},$$

$$\mathbf{A} = \left[\begin{array}{cc} k_n \sinh k_n L_1 & k_n \sinh k_n L_2 \\ k_n \sinh k_n L_1 + i\omega\beta \cosh k_n L_1 & -i\omega\beta \cosh k_n L_2 \end{array} \right].$$

This system of equations has a unique solution if $\det(\mathbf{A}) \neq 0$ where

$$\det(\mathbf{A}) = -k_n^2 \sinh k_n L_1 \sinh k_n L_2 \Delta_n, \quad \Delta_n = 1 + \frac{i\omega\beta}{k_n}[\coth k_n L_1 + \coth k_n L_2].$$

This expression is zero if $k_n = 0$, which we can discard as a translation of the system, or $\sinh k_n L_1 = \sinh k_n L_2 = 0$, or if $\Delta_n = 0$. The $\sinh k_n L_1 = \sinh k_n L_2 = 0$ case corresponds to k_n being purely imaginary, which in fact corresponds to this mode being associated with the wave mode for ω real, and hence is just a reordering of the eigenvalues. The third case leads to the trivial solution for B_{jn}. Therefore we can consider the case $\det(\mathbf{A}) \neq 0$ and deal with the above cases later. Assuming $\det(\mathbf{A}) \neq 0$, inverting the coefficient matrix $\mathbf{A}$, and solving gives

$$B_{jn} = \frac{(-1)^j}{k_n^2 |\Delta_n|^2} \left[-\omega^2 \beta c_n \frac{\tanh \frac{1}{2} k_n L_1 + \tanh \frac{1}{2} k_n L_2}{\sinh k_n L_j} \right.$$
$$\left. + i\left(\omega c_n k_n \tanh \frac{1}{2} k_n L_j + \frac{\omega^3 \beta^2 c_n}{k_n} \tanh \frac{1}{2} k_n(L_1 + L_2)(\coth k_n L_1 + \coth k_n L_2)^2 \right) \right] \widehat{q}, \tag{2.37}$$

for $j = 1, 2$ and $n \geq 1$.

Next we consider the first pair of equations (2.33) and (2.34), which too can be written in matrix form $\widehat{\mathbf{A}}\widehat{\mathbf{b}} = \widehat{\mathbf{q}}$, for the parameters $\widehat{\mathbf{b}} = (B_{10}, B_{20})^T$ with

$$\widehat{\mathbf{q}} = \omega c_0 \left[\begin{array}{c} -i(\cos k_0 L_2 - \cos k_0 L_1) \\ i(\cos k_0 L_1 - 1) - \frac{\beta\omega}{k_0}(\sin k_0 L_1 + \sin k_0 L_2) \end{array} \right] \widehat{q},$$

$$\widehat{\mathbf{A}} = \left[\begin{array}{cc} k_0 \sin k_0 L_1 & k_0 \sin k_0 L_2 \\ k_0 \sin k_0 L_1 - i\omega\beta \cos k_0 L_1 & i\beta\omega \cos k_0 L_2 \end{array} \right]. \tag{2.38}$$

Again we have a unique solution if $\det(\widehat{\mathbf{A}}) \neq 0$ where

$$\det(\widehat{\mathbf{A}}) = -k_0^2 \sin k_0 L_1 \sin k_0 L_2 \Delta_0, \quad \Delta_0 = 1 - \frac{\mathrm{i}\omega\beta}{k_0}\left[\cot k_0 L_1 + \cot k_0 L_2\right].$$

In this case $\det(\widehat{\mathbf{A}}) = 0$ if $\sin k_0 L_1 = \sin k_0 L_2 = 0$ simultaneously (again neglecting $k_0 = 0$), which occurs if

$$k_0 L_1 = m\pi \quad \text{and} \quad k_0 L_2 = m'\pi,$$

for $m, m' \in \mathbb{Z}$, and thus means the lengths of the two compartments must satisfy $mL_2 = m'L_1$. These solutions correspond to symmetric free-sloshing modes with $k_0 \in \mathbb{R}$. Also $\det(\widehat{\mathbf{A}})$ could be zero if $\Delta_0 = 0$, i.e. $\omega = -\mathrm{i}k_0/(\beta(\cot k_0 L_1 + \cot k_0 L_2))$, but this again leads to the trivial solution. See Appendix A for more on these solutions.

Making the observation that $\det(\widehat{\mathbf{A}})$ could be zero, then (2.33) and (2.34) essentially become two equations which couple the three unknowns B_{10}, B_{20} and $\widehat{q}$. A third equation linking these constants comes from the vessel equation (2.24). Substituting in the normal mode forms (2.18) and evaluating the integrals by using the fact that the vertical eigenmodes satisfy

$$\int_0^H \psi_0(y)\,\mathrm{d}y = Hc_0 \quad \text{and} \quad \int_0^H \psi_n(y)\,\mathrm{d}y = Hc_n,$$

leads to the vessel equation

$$\mathrm{i}\omega\rho Hc_0(\cos k_0 L_1 - 1)B_{10} + \mathrm{i}\omega\rho Hc_0(1 - \cos k_0 L_2)B_{20} + \Theta\widehat{q} = 0, \qquad (2.39)$$

where

$$\Theta = -\frac{\omega^2 \rho Hc_0^2}{k_0}(\sin k_0 L_1 + \sin k_0 L_2) + \widehat{\Theta}_0 + \beta^2\widehat{\Theta}_1 - \beta\mathrm{i}\widehat{\Theta}_2, \qquad (2.40)$$

and

$$\widehat{\Theta}_0 = \nu - m_v\omega^2 - 2\omega^2\rho H\sum_{n=1}^{\infty}\frac{c_n^2}{k_n|\widehat{\Delta}_n|^2}\left(\tanh\frac{1}{2}k_nL_1 + \tanh\frac{1}{2}k_nL_2\right),$$

$$\widehat{\Theta}_1 = -2\omega^4\rho H\sum_{n=1}^{\infty}\frac{c_n^2}{k_n^3|\widehat{\Delta}_n|^2}\tanh\frac{1}{2}k_n(L_1 + L_2)\left(\coth k_nL_1 + \coth k_nL_2\right)^2,$$

$$\widehat{\Theta}_2 = -\omega^3\rho H\sum_{n=1}^{\infty}\frac{c_n^2}{k_n^2|\widehat{\Delta}_n|^2}\left[\tanh\frac{1}{2}k_nL_1 + \tanh\frac{1}{2}k_nL_2\right]^2.$$

The three equations (2.33), (2.34) and (2.39) define 3 equations for the 3 unknowns B_{10}, B_{20} and $\widehat{q}$, which by seeking a non-trivial solution, yields an eigenvalue problem for ω.

2.3   The Characteristic Equation

The characteristic equation for the unknown frequency ω is found by identifying non-trivial solutions to (2.33), (2.34) and (2.39). The equations can be written as the matrix problem

$$\mathbf{Tz} = \mathbf{0}, \qquad (2.41)$$

9

where,

$$\mathbf{T} = \begin{bmatrix} k_0 \sin k_0 L_1 & k_0 \sin k_0 L_2 & \mathrm{i}\omega c_0(\cos k_0 L_2 - \cos k_0 L_1) \\ k_0 \sin k_0 L_1 - \mathrm{i}\omega\beta \cos k_0 L_1 & \mathrm{i}\omega\beta \cos k_0 L_2 & -\omega c_0 \zeta \\ \mathrm{i}\omega\rho H c_0(\cos k_0 L_1 - 1) & \mathrm{i}\omega\rho H c_0(1 - \cos k_0 L_2) & \Theta \end{bmatrix},$$

$$\mathbf{z} = \begin{bmatrix} B_{10} & B_{20} & \widehat{q} \end{bmatrix}^T,$$

and

$$\zeta = \mathrm{i}(\cos k_0 L_1 - 1) - \frac{\omega\beta}{k_0}(\sin k_0 L_1 + \sin k_0 L_2).$$

Non-trivial solutions occur when the determinant of the coefficient matrix is zero, which leads to the characteristic equation

$$\begin{aligned} D(\omega) &= 2k_0\omega^2 H\rho c_0^2 \sin k_0 L_1 \sin k_0 L_2 \left[\tan \frac{1}{2}k_0 L_1 + \tan \frac{1}{2}k_0 L_2 \right] \\ &\quad -2\mathrm{i}\beta\omega^3 H\rho c_0^2 \left[1 - \cos k_0(L_1 + L_2) \right] \\ &\quad -(\widehat{\Theta}_0 + \beta^2\widehat{\Theta}_1 - \mathrm{i}\beta\widehat{\Theta}_2) \left[k_0^2 \sin k_0 L_1 \sin k_0 L_2 - \mathrm{i}\omega\beta k_0 \sin k_0(L_1 + L_2) \right], \end{aligned}$$

which is solved for the unknown frequencies ω. There are an infinite number of natural frequencies, and once each is calculated, the corresponding eigenvector $(B_{10}, B_{20}, \widehat{q})^T$ gives the ratios of the unknown amplitudes. In appendix A we show that the symmetric free-sloshing modes, when $\sin k_0 L_1 = \sin k_0 L_2 = 0$, occur when the vessel is at rest ($\widehat{q} \equiv 0$). Here the constants satisfy $B_{10} = B_{20}$ and are arbitrary, being fixed by the initial conditions. In the case of non-symmetric sloshing modes when $\det(\widehat{\mathbf{A}}) \neq 0$ then we can solve for B_{10} and B_{20} as a function of $\widehat{q}$ as

$$\begin{aligned} B_{j0} &= \frac{(-1)^j}{k_0^2 |\Delta_0|^2} \left[\omega^2 \beta c_0 \frac{\tan \frac{1}{2}k_0 L_1 + \tan \frac{1}{2}k_0 L_2}{\sin k_0 L_j} \right. \\ &\quad \left. +\mathrm{i} \left(\omega c_0 k_0 \tan \frac{1}{2}k_0 L_j + \frac{\omega^3 \beta^2 c_0}{k_0} \tan \frac{1}{2}k_0(L_1 + L_2) \left(\cot k_0 L_1 + \cot k_0 L_2 \right)^2 \right) \right] \widehat{q}, \end{aligned}$$

(2.42)

where $\widehat{q}$ is dependent on the initial conditions. Hence, as in (2.37), the value of B_{j0} couples to the vessel motion.

2.4 Non-dimensionalisation

The characteristic equation (2.42) contains many physical parameters, but the number of these parameters can be reduced by considering the non-dimensional form of the system. We non-dimensionalise the system of equations based on the non-dimensionalisation first set out by [43]. Here we define the non-dimensional quantities as

$$R = \frac{m_v}{m_f}, \quad G = \frac{\nu(L_1 + L_2)^2}{4gH m_f}, \quad s = \frac{\omega(L_1 + L_2)}{2\sqrt{gH}}, \quad \gamma = 2\sqrt{gH}\beta,$$

$$\alpha_n = k_n(L_1 + L_2), \quad \mu_1 = \frac{L_1}{L_1 + L_2} = \mu, \quad \mu_2 = \frac{L_2}{L_1 + L_2} = 1 - \mu,$$

$$C_{jk} = \frac{B_{jk}}{2\sqrt{gH}(L_1 + L_2)}, \quad Q = \frac{\widehat{q}}{L_1 + L_2},$$

where we define the fluid mass as $m_f = \rho H(L_1 + L_2)$. Then the characteristic equation becomes

$$
\begin{aligned}
D(s) &= 2\alpha_0 s^2 c_0^2 \sin \alpha_0 \mu \sin \alpha_0 (1-\mu) \left[\tan \frac{1}{2} \alpha_0 \mu + \tan \frac{1}{2} \alpha_0 (1-\mu) \right] - 2\mathrm{i}\gamma s^3 c_0^2 \left[1 - \cos \alpha_0 \right] \\
&\quad - (\Theta_0 + \gamma^2 \Theta_1 - \mathrm{i}\gamma \Theta_2) \left[\alpha_0^2 \sin \alpha_0 \mu \sin \alpha_0 (1-\mu) - \mathrm{i}s\gamma \alpha_0 \sin \alpha_0 \right],
\end{aligned}
\tag{2.43}
$$

where we define

$$
\begin{aligned}
\Theta_0 &= G - Rs^2 - 2s^2 \sum_{n=1}^{\infty} \frac{c_n^2}{\alpha_n |\Delta_n|^2} \left(\tanh \frac{1}{2} \alpha_n \mu + \tanh \frac{1}{2} \alpha_n (1-\mu) \right), \\
\Theta_1 &= -2s^4 \sum_{n=1}^{\infty} \frac{c_n^2}{\alpha^3 |\Delta_n|^2} \tanh \frac{1}{2} \alpha_n \left(\coth \alpha_n \mu + \coth \alpha_n (1-\mu) \right)^2, \\
\Theta_2 &= -s^3 \sum_{n=1}^{\infty} \frac{c_n^2}{\alpha_n |\Delta_n|^2} \left(\tanh \frac{1}{2} \alpha_n \mu + \tanh \frac{1}{2} \alpha_n (1-\mu) \right)^2,
\end{aligned}
\tag{2.44}
$$

and

$$
|\Delta_n|^2 = 1 + \frac{\gamma^2 s^2}{\alpha_n^2} \left[\coth \alpha_n \mu + \coth \alpha_n (1-\mu) \right]^2.
$$

The eigenvalues α_n for $n \geq 0$ are found from (2.26) and (2.27) which in non-dimensional form are

$$
\alpha_0 \tanh \alpha_0 \delta - 4\delta s^2 = 0, \quad \text{and} \quad \alpha_n \tan \alpha_n \delta + 4\delta s^2 = 0,
\tag{2.45}
$$

where $\delta = H/(L_1 + L_2)$ is the non-dimensional fluid depth parameter.

For cases when $\det(\widehat{\mathbf{A}}) \neq 0$ the non-dimensional forms of the amplitude parameters (2.42) and (2.37) become

$$
\begin{aligned}
C_{j0} &= \frac{(-1)^j}{\alpha_0^2 |\Delta_0|^2} \left[s^2 \gamma c_0 \frac{\tan \frac{1}{2}\alpha_0 \mu + \tan \frac{1}{2}\alpha_0(1-\mu)}{\sin \alpha_0 \mu_j} \right. \\
&\quad \left. + \mathrm{i} \left(s c_0 \alpha_0 \tan \frac{1}{2}\alpha_0 \mu_j + \frac{s^3 \gamma^2 c_0}{\alpha_0} \tan \frac{1}{2}\alpha_0 \left(\cot \alpha_0 \mu + \cot \alpha_0(1-\mu) \right)^2 \right) \right] Q,
\end{aligned}
\tag{2.46}
$$

$$
\begin{aligned}
C_{jn} &= \frac{(-1)^j}{\alpha_n^2 |\Delta_n|^2} \left[-s^2 \gamma c_n \frac{\tanh \frac{1}{2}\alpha_n \mu + \tanh \frac{1}{2}\alpha_n(1-\mu)}{\sinh \alpha_n \mu_j} \right. \\
&\quad \left. + \mathrm{i} \left(s c_n \alpha_n \tanh \frac{1}{2}\alpha_n \mu_j + \frac{s^3 \gamma^2 c_n}{\alpha_n} \tanh \frac{1}{2}\alpha_n \left(\coth \alpha_n \mu + \coth \alpha_n(1-\mu) \right)^2 \right) \right] Q,
\end{aligned}
\tag{2.47}
$$

respectively, for $j = 1, 2$, where

$$
|\Delta_0|^2 = 1 + \frac{\gamma^2 s^2}{\alpha_0^2} \left[\cot \alpha_0 \mu + \cot \alpha_0(1-\mu) \right]^2.
$$

The characteristic equation (2.43) can be shown to reduce to the equation presented in [35] when $|\gamma| \to \infty$ and to the two compartment relation in [7] when $|\gamma| = 0$. We show this explicitly in appendix B where we calculate the first two terms of the asymptotic solutions for s in the limits $\gamma \to 0$ and $\gamma \to \infty$ with $\gamma \in \mathbb{R}$.

2.5 Shallow-Water Limit

In the shallow-water limit the depth parameter $\delta \ll 1$, with all other parameters held fixed. The eigenvalues related to the vertical eigenfunctions satisfy (2.45), the first of which describes the wave mode. In the limit $\delta \to 0$ then

$$4\delta^2 s^2 = \alpha_0^2 \delta^2 - \frac{1}{3}\alpha_0^4 \delta^4 + O(\delta^6),$$

which at leading order gives

$$s = \frac{1}{2}\alpha_0.$$

For the evanescent modes, we observe that each solution must lie in the range $(n-1)\pi < \mathrm{Re}(\alpha_n \delta) < n\pi$, thus it can be shown that

$$\alpha_n \delta = n\pi - \frac{\alpha_0^2 \delta^2}{n\pi} + O(\delta^4).$$

Substituting these approximations into the coefficients c_0 and c_n we find that the leading order terms satisfy

$$c_0 = 1 + O(\delta^4), \quad \text{and} \quad c_n = O(\delta^2).$$

Hence in the shallow-water limit the evanescent modes are $O(\delta^2)$ smaller in magnitude to the wave mode, and at leading order the characteristic equation can be written solely in terms of the frequency s as

$$
\begin{aligned}
D^{\mathrm{SW}}(s) \;=\;& 4s^2 \sin 2\mu s \sin 2(1-\mu)s \left[s \tan \mu s + s \tan(1-\mu)s - G + Rs^2 \right] \\
& -2\mathrm{i}\gamma s^2 \sin 2s \left[s \tan s - G + Rs^2 \right].
\end{aligned}
\tag{2.48}
$$

In this limit the form of the characteristic equation is the sum of the two compartment shallow-water equation from [7] and the one compartment shallow-water equation from the work of [35] with an $\mathrm{i}\gamma$ prefactor. Hence it is clear that this equation gives the correct characteristic equations in the limits $|\gamma| = 0$ and $|\gamma| \to \infty$, and there is a linear transition between the two cases as γ varies.

3 Results

3.1 Single Baffle System

In this section we consider numerical solutions to the non-dimensional form of the characteristic equation for both finite, (2.43), and shallow depth, (2.48), fluids. In both cases the unknown complex frequency s is found via Newton iterations with the mth update for s given by

$$s^{m+1} = s^m - \frac{D(s^m)}{D'(s^m)},$$

where the dash denotes differentiation with respect to s. For the initial guesses for s^0 we use either results from the $|\gamma| = 0$ or $|\gamma| \to \infty$ limits, as here $s \in \mathbb{R}$ and we can identify s^0 visually by plotting $D(s)$ and manually looking for the roots. Iterations are continues until $|s^{m+1} - s^m| < 10^{-8}$. From these results we use parameter continuation techniques on γ to find values of s at finite values of γ, both real and complex. The complex eigenvalues α_n are identified by solving (2.45) iteratively via Newton iterations,

and noting that $(n-1)\pi < \mathrm{Re}(\alpha_n \delta) < n\pi$ so as to make sure we capture all the solutions. The infinite sums in (2.44) are truncated at 40 evanescent modes, which give converged results for all parameter sets considered. The initial guesses for α_n are found by solving the vertical eigenvalue problem given in [35] directly by expanding the solution as a series of Chebyshev polynomials. This is discussed in detail in [35].

Initially we focus on two vessel configurations, a symmetric configuration with $\mu = 0.5$ and an asymmetric configuration with $\mu = 0.3$, with $\gamma \in \mathbb{R}$. In figure 2 we consider the
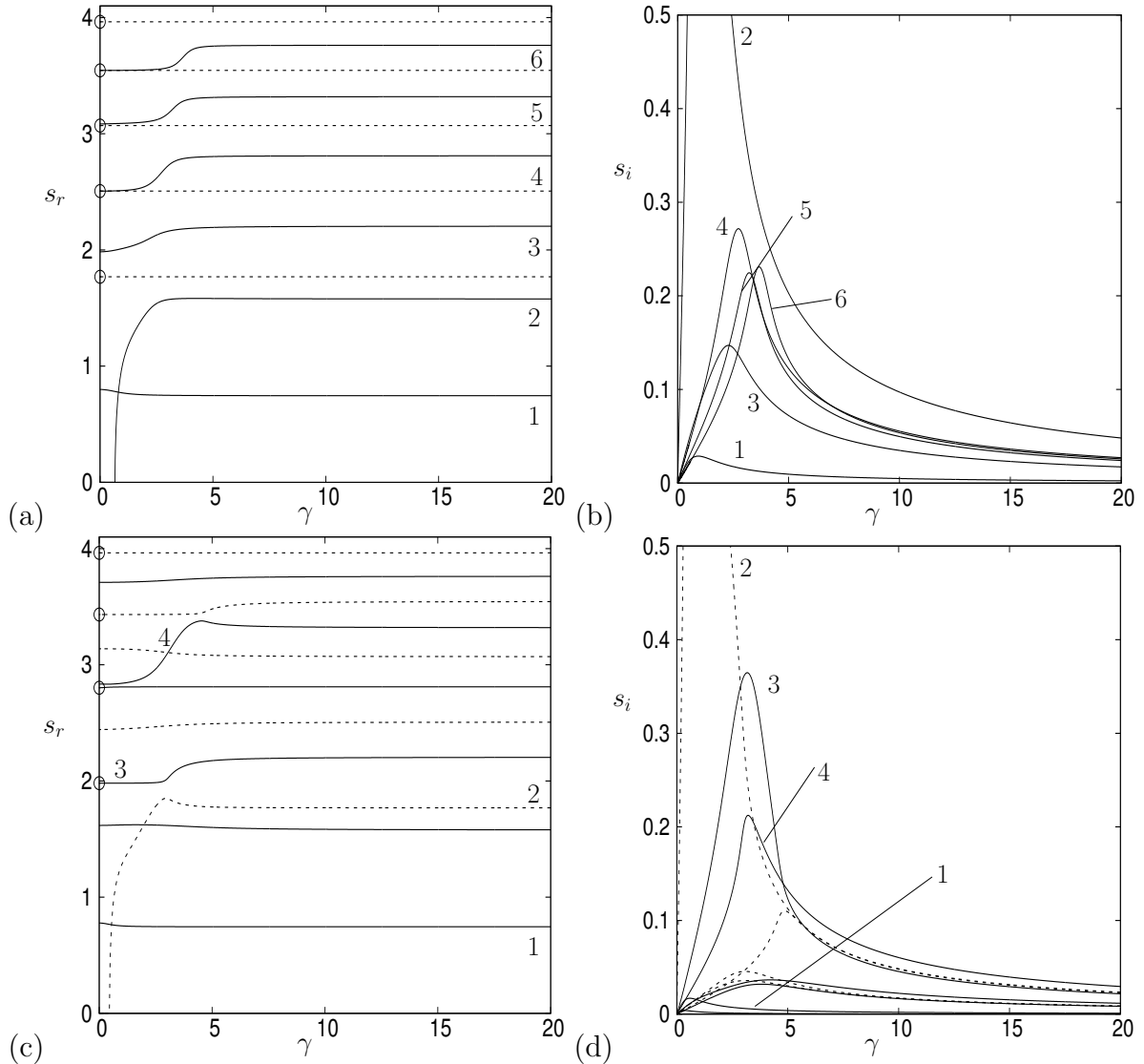
Figure 2: Plots of $s_r(\gamma)$ and $s_i(\gamma)$ from (2.43) for $(G, R, \delta) = (1, 0.5, 0.5)$ and (a,b) $\mu = 0.5$ and (c,d) $\mu = 0.3$. The dashed lines represent modes which are symmetric modes in a stationary vessel ($Q = 0$) in the limit $\gamma \to \infty$. The circles at $\gamma = 0$ signify symmetric sloshing modes in this limit.

variation of the real and imaginary parts of $s = s_r + \mathrm{i}s_i$ as a function of γ for parameters $(G, R, \delta) = (1, 0.5, 0.5)$ and (a,b) $\mu = 0.5$ and (c,d) $\mu = 0.3$. In this figure the solid lines represent modes which are anti-symmetric sloshing modes (which couple to a moving vessel) in the $\gamma \to \infty$ limit, while the dashed lines represent symmetric modes (i.e. which exist in a stationary vessel), in the $\gamma \to \infty$ limit. The circles at $\gamma = 0$ show the frequencies

of the symmetric sloshing modes in the $\gamma = 0$ limit. For the $\mu = 0.5$ configuration in panels (a,b), we observe that the symmetric modes remain symmetric modes as the wall porosity parameter γ is varied, with a fixed s_r value and $s_i = 0$. This means that these modes remain neutral modes, and the vessel remains stationary, i.e. $Q = 0$ as γ varies. In these cases the free-surface profile is similar to that given in figure 11 of Appendix A, where the fluid generates an equal and opposite force on the vessel walls and the baffle, resulting in no net force on the vessel.

The solid lines, representing the anti-symmetric modes, couple to the vessel motion, hence $Q \neq 0$. Here we see that for $\gamma \gtrsim 5$ these modes appear to have a constant value of s_r equal to the $\gamma \to \infty$ limit result, but in panel (b) we see these modes have $s_i > 0$, meaning these modes are exponentially decaying modes. For $\gamma \in [0, 5]$ the frequency (real part of the complex frequency) of these modes rapidly varies from the $\gamma \to \infty$ result to the $\gamma = 0$ result. In this region the corresponding decay rate s_i reaches its maximum value for each of these modes, hence the maximal damping of the system occurs when s_r varies the greatest. A similar conclusion was found for the lowest sloshing mode only in the model of [44]. The ordering of the decay rates is not directly related to the value of s_r, i.e. larger s_r values do not necessary decay faster/slower than modes with smaller s_r values. In particular in figure 2, we observe that it is the mode labeled 2 which decays fastest in this system. When this mode intersects with $s_r = 0$ there is a bifurcation into two unstable modes with $s_r = 0$ and $s_i \neq 0$. The reason for this is due to two modes with $s_r = S(\gamma)$ and $s_r = -S(\gamma)$ interacting at $s_r = 0$. When $s_r = 0$ for these two modes, they become unstable modes in a stationary vessel, and hence are not of significance in this study, as our main interest is in modes which are coupled to the vessel motion. One thing we do observe in this figure is that the lowest frequency mode as $\gamma \to \infty$ remains the lowest frequency mode as $\gamma \to 0$ (except for a tiny range of γ values where the mode labeled 2 goes to zero).

When we consider the $\mu = 0.3$ non-symmetric vessel configuration in panels (c,d) we observe that the symmetric sloshing modes (in either the $\gamma = 0$ or $\gamma \to \infty$ limits) are no longer neutral for all values of γ, and now decay except in these two limits. Also the value of s_r now varies as γ varies, i.e. they no longer have constant frequency. The overall behaviour of the mode frequencies, s_r, is similar to the $\mu = 0.5$ case, with the variations in both the real and imaginary parts of s occurring mainly for $0 \leq \gamma \leq 5$, and with similar magnitude decay rates. We again observe a mode (labeled 2) which as $\gamma \to 0$ we find $s_r = 0$ for small γ. The difference in this case is this mode is a symmetric mode, in a stationary vessel, in the $\gamma \to \infty$ limit, not an anti-symmetric mode. We now also observe modes which switch type in the two extremes of γ, such as that labeled 3 in panel (c). This mode is an anti-symmetric mode as $\gamma \to \infty$, but as γ is reduced it becomes a symmetric mode at $\gamma = 0$.

As δ is reduced to $\delta = 0.1$ (again with $(G, R) = (1, 0.5)$) in figure 3, i.e. as we move closer to the shallow-water limit, we find that the higher frequency modes, s_r, become more distinct, i.e. more spread out, as do the decay rates, s_i, of the modes. As a general observation, it appears that the maximum decay rates increase in magnitude as δ is increased. This is particularly apparent in the $\mu = 0.3$ configuration. It is however, still the case that the majority of the variation in s is restricted to the region $\gamma \lesssim 5$.

In appendix B we calculate the asymptotic form of s in the limits $\gamma \to 0$ and $\gamma \to \infty$ with $\gamma \in \mathbb{R}$. In figure 4 these approximations (dashed lines) are compared to the full numerical result (solid lines), and we observe excellent agreement in both these limits, despite both s_r and s_i each containing only one term in their expansions. However,
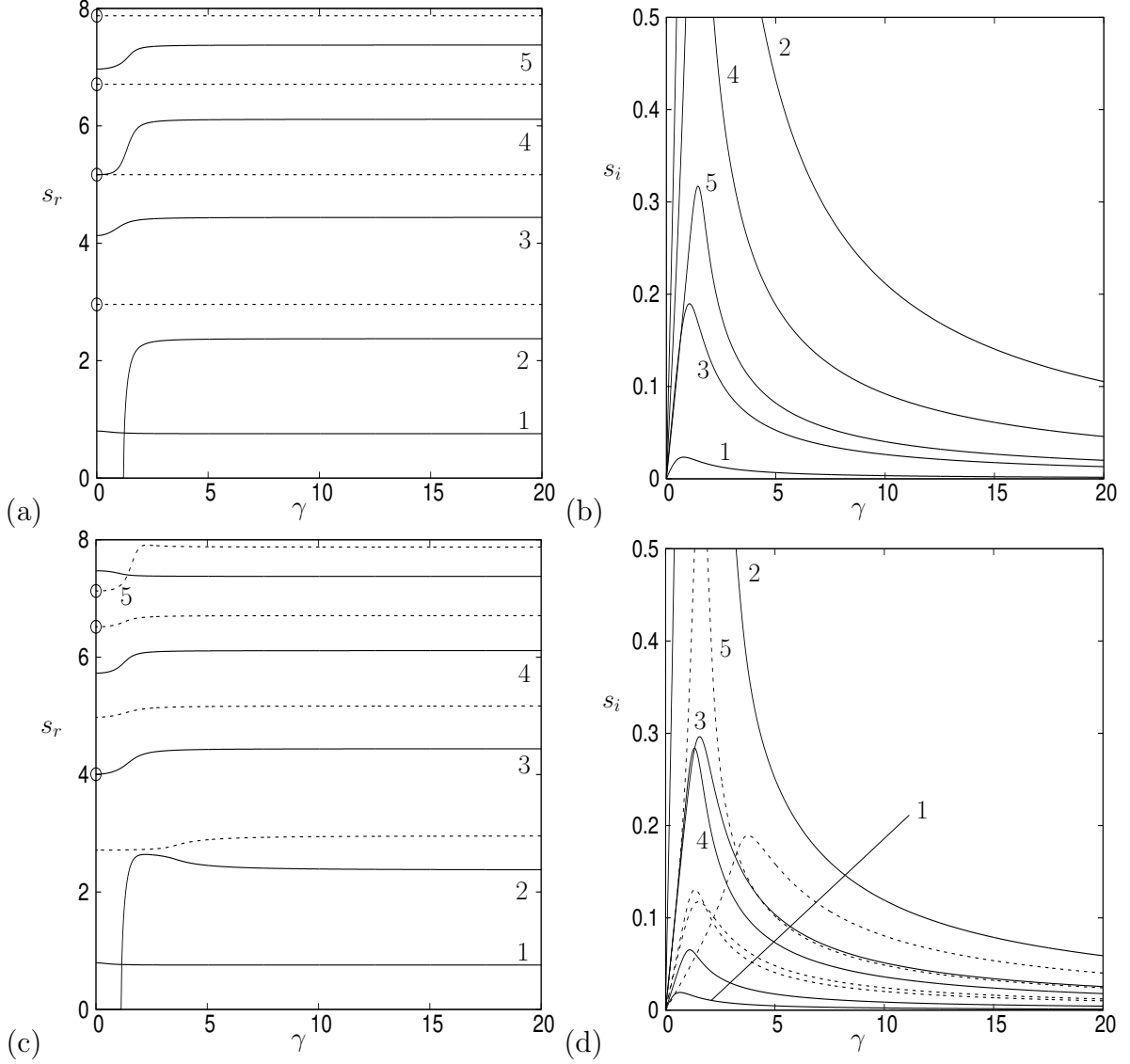
Figure 3: Plots of $s_r(\gamma)$ and $s_i(\gamma)$ from (2.43) for $(G, R, \delta) = (1, 0.5, 0.1)$ and (a,b) $\mu = 0.5$ and (c,d) $\mu = 0.3$. The dashed lines represent modes which are symmetric modes in a stationary vessel $(Q = 0)$ in the limit $\gamma \to \infty$. The circles at $\gamma = 0$ signify symmetric sloshing modes in this limit.

this level of approximation is not able to capture the maximum decay rate of the modes accurately, although it does allow for predictions of the system's decay in the two extreme limits, along with an approximate maximum growth rate where the two approximations intersect. This would be of particular interest if the baffle porosity were time dependent, with sloshing waves generated with $\gamma = 0$ and then the baffle porosity was varied. The initial rate of decay of the system could then be accurately predicted by the asymptotic results, especially if the variation was slow.

In figure 5 we consider the form of $s = s_r + \mathrm{i}s_i$ when $\mu = 0.5$ (with $(G, R, \delta) = (1, 0.5, 0.5)$) when $\gamma = \gamma_r(1 + 0.1\mathrm{i})$. Here the imaginary part of γ represents the inertial effect of the fluid in the baffle, and is typically smaller than the real part [41]. The results with $\gamma \in \mathbb{C}$, given by the solid lines, are compared to the equivalent results with $\gamma = \gamma_r \in \mathbb{R}$ from figure 2(a,b). What this figure shows is the inclusion of inertial effects
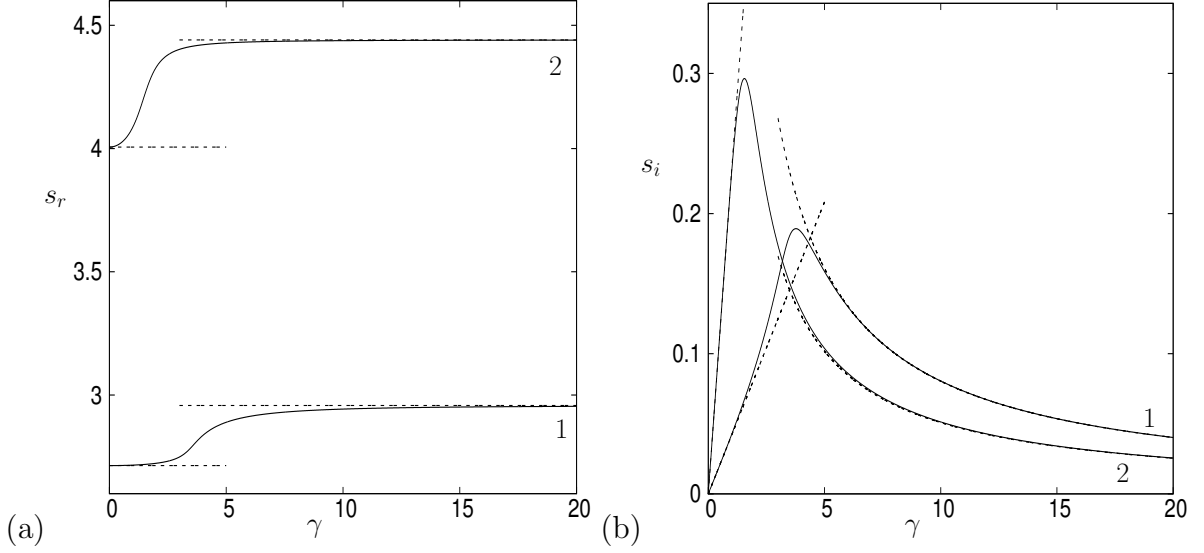
Figure 4: Plot of $s_r(\gamma)$ and $s_i(\gamma)$ for two modes from figure 3 with $(G, R, \delta, \mu) = (1, 0.5, 0.1, 0.3)$. The solid lines give the numerical solutions of (2.43) while the dashed lines give the asymptotic results calculated in Appendix B
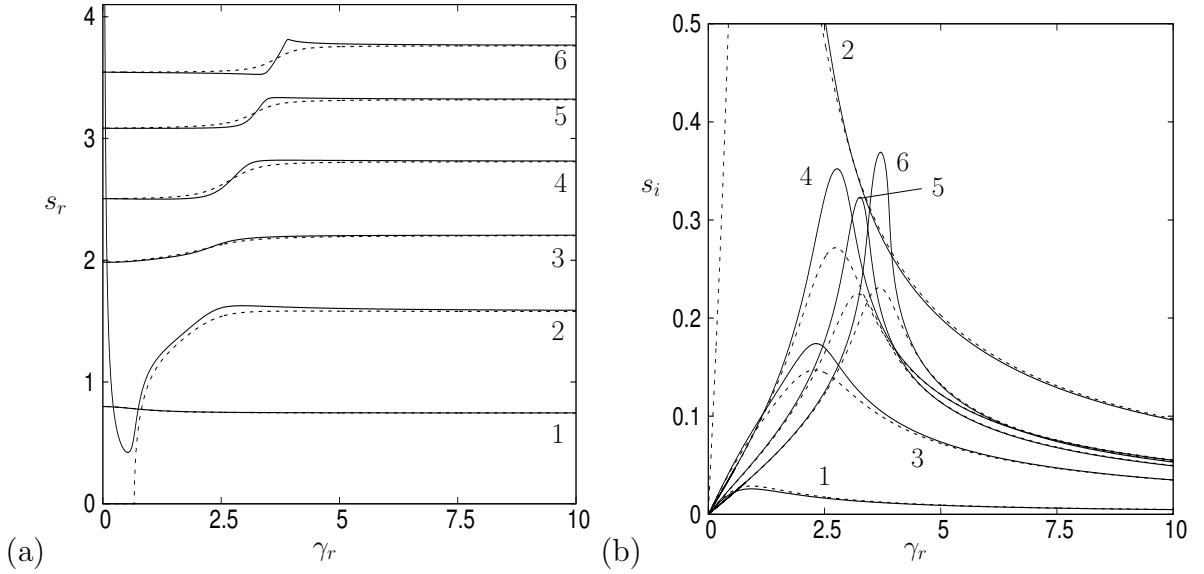

Figure 5: Plots of $s_r(\gamma_r)$ and $s_i(\gamma_r)$ from (2.43) for $(G, R, \delta) = (1, 0.5, 0.5)$ and $\mu = 0.5$. Here $\gamma = \gamma_r(1 + 0.1i)$. The solid lines are the values of s_r and s_i for the complex value of γ, while the dashed lines are the corresponding result with $\gamma = \gamma_r$, as given in figure 2(a,b).

typically increases the decay rate, s_i, of the system for the higher frequency modes, but makes a relatively modest modification to the lowest frequency mode. The larger peaks in s_i in figure 5(b) are accompanied by sharper changes in the corresponding s_r value in figure 5(a). The other obvious change in this case compared to figure 2 is that the s_r value for mode 2 now does not go to zero, where it interacted with a second mode, and instead $s_r \to \infty$ as $\gamma_r \to 0$.

In the shallow-water limit, the characteristic equation simplifies to (2.48) and the
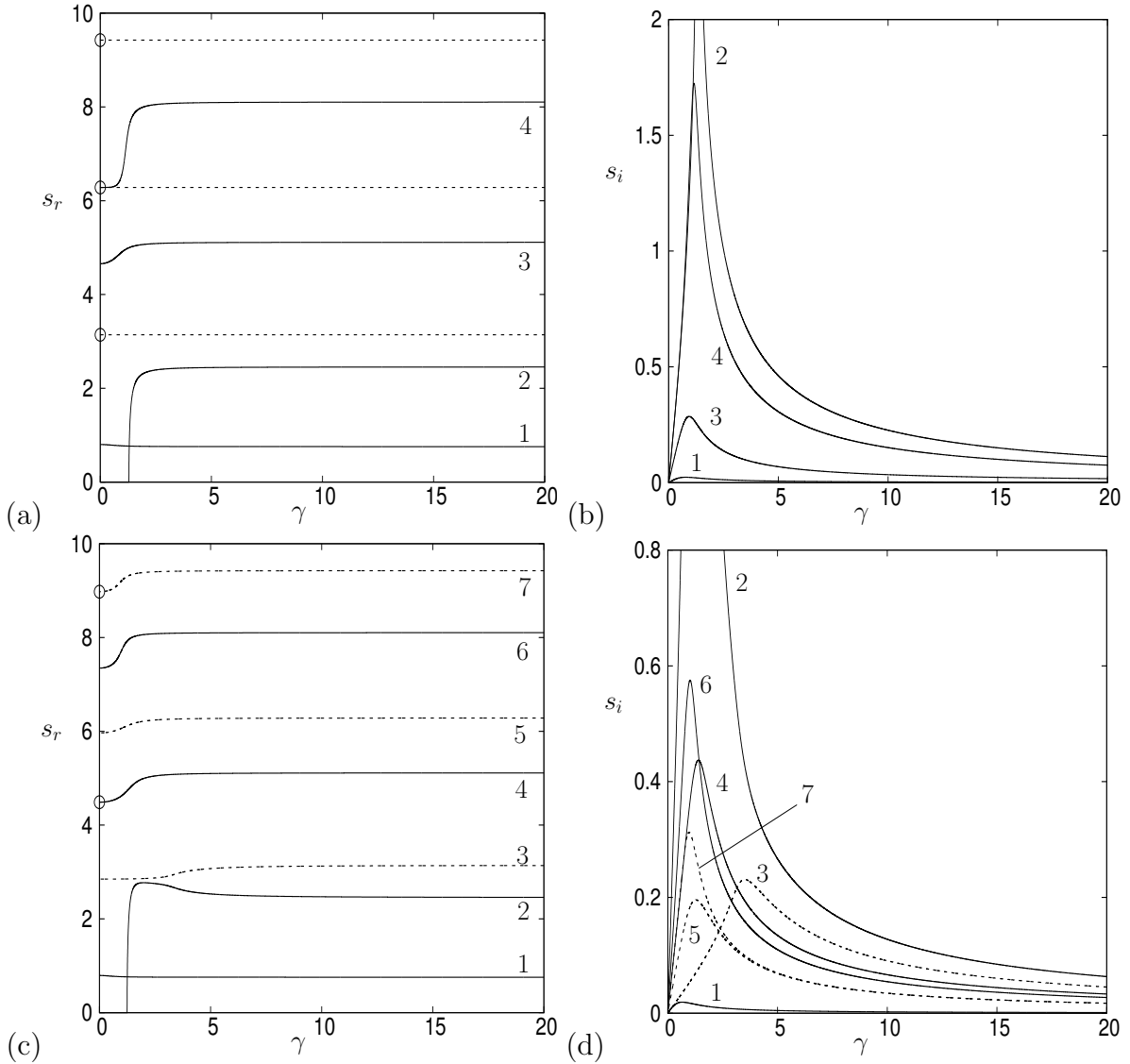
Figure 6: Plots of $s_r(\gamma)$ and $s_i(\gamma)$ in the shallow-water limit from (2.48) for $(G, R) = (1, 0.5)$ and (a,b) $\mu = 0.5$ and (c,d) $\mu = 0.3$. The dashed lines represent modes which are symmetric modes in a stationary vessel $(Q = 0)$ in the limit $\gamma \to \infty$. The circles at $\gamma = 0$ signify symmetric sloshing modes in this limit.

solutions to this equation, plotted in figure 6, are found to agree well with those in figure 3, at least for the smaller frequency results. The main benefit of the shallow-water approximation is that the values of s can be calculated more easily (i.e. without calculating the intermediary eigenvalues α_n). Also, in systems where the lower frequency modes dominate, and the higher frequency modes can be neglected, then the shallow-water approximation is beneficial due to the speed of computation.

A typical initial condition for an experimental setup for the system in figure 1, such as extending the spring and releasing the vessel from a stationary position, would consist of a superposition of these individual modes. However, unlike for the impermeable baffle problem, where all modes are undamped and so persist for all times, the higher frequency modes are typically damped out fastest, and so in this experimental setup we would expect the lowest frequency mode (as it is the least damped) to be the most significant.

17

Also, following [36] the coefficient of the lowest frequency mode tends to have the largest amplitude in the eigenmode expansion for most initial conditions. Thus we focus our attention in the remainder of the paper on the lowest frequency mode in the shallow-water limit.
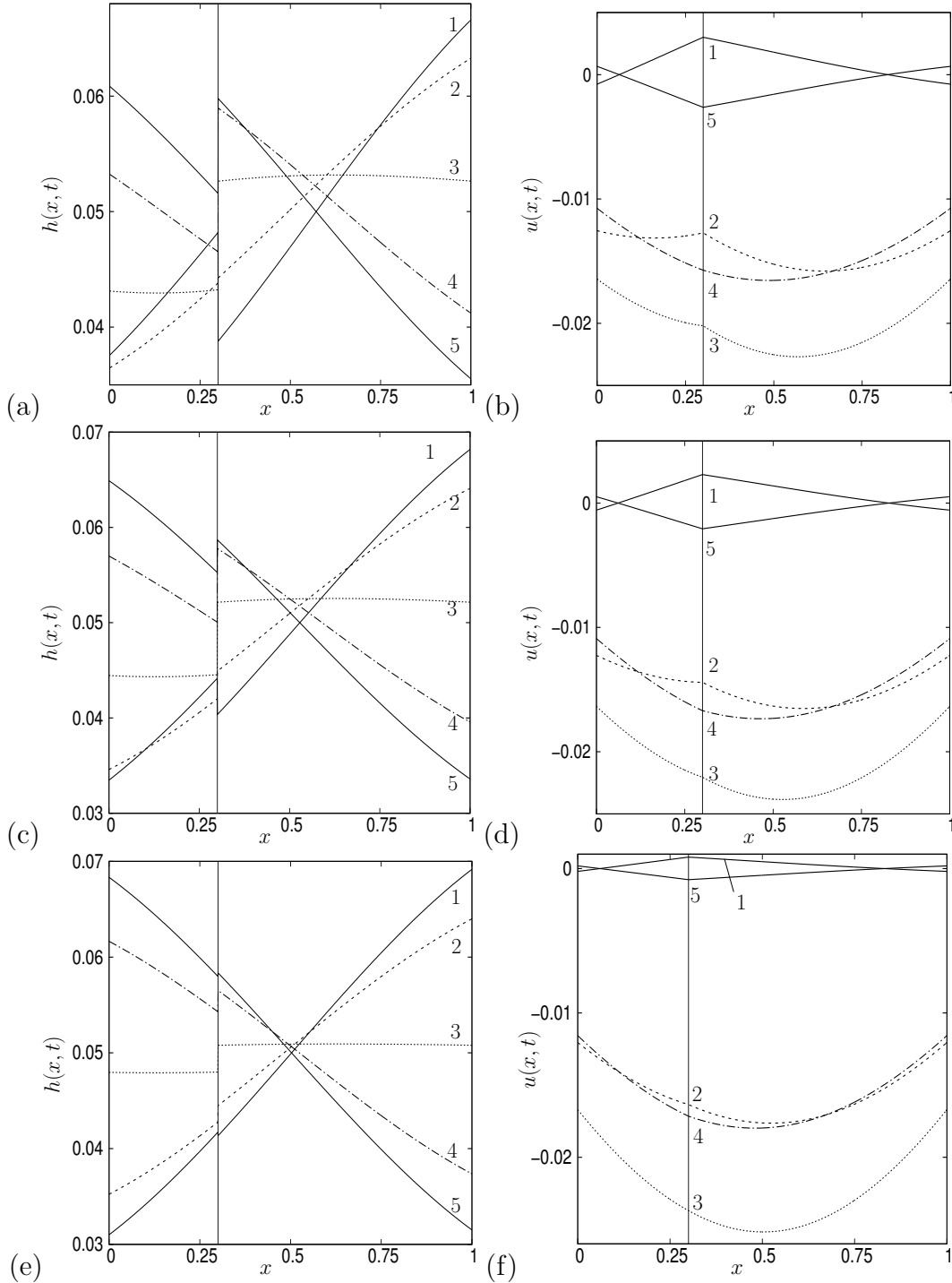

Figure 7: Plot of the non-dimensional free-surface elevation $h_j(x,t)$ and horizontal velocity component $u_j(x,t) = \phi_x(x,t)$ for $j = 1, 2$ in the shallow-water limit for $(G, R, \delta, \mu, \epsilon) = (1, 0.5, 0.05, 0.3, 0.01)$ at times $t/(2s_r) = 0, \frac{\pi}{4}, \frac{\pi}{2}, \frac{3\pi}{4}, \pi$ numbered 1-5 respectively. In (a,b) $\gamma = 0.8$, (c,d) $\gamma = 1.5$, while in (e,f) $\gamma = 5$.

18

In figure 7 we consider the time evolution of the non-dimensional free-surface profiles $h_j(x,t)$ and horizontal velocity $u_j(x,t)$ for the lowest frequency mode in the shallow-water limit for $(G, R, \delta) = (1, 0.5, 0.05)$ with (a,b) $\gamma = 0.8$, (c,d) $\gamma = 1.5$ and (e,f) $\gamma = 5$. The form of the free-surface profile can be found from (2.12) which when non-dimensionalised is given by

$$h_j(x,t) = \delta - \left[2i\epsilon s A_{j0}(x) e^{2ist} + \text{c.c} \right], \tag{3.49}$$

while the non-dimensional horizontal velocity in the fixed reference frame is given by

$$u_j(x,t) = \frac{\partial \phi_j}{\partial x} = \epsilon \frac{\partial A_{j0}}{\partial x}(x) e^{2ist} + \text{c.c}, \tag{3.50}$$

where c.c denotes the complex conjugate. Here $j = 1, 2$ denotes the two separate regions of the vessel. The wave mode is the driving mode in the system, and hence plotting $h(x,t)$ and $u(x,t)$ without the evanescent modes provides excellent notion for the fluid motion. The evanescent modes provide a perturbation to this result, typically reducing the fluid height, $h(x,t)$, at the side walls and baffle, and increasing it in the interior of the fluid. This was demonstrated for the zero-baffle problem in [35].

In panels (a,b) the baffle has a low porosity value and so there is a delay in the fluid flowing between each region, resulting in the average fluid depth in each region being significantly different at each time value, e.g. result 3 at $t = \pi s_r$. There is also a very clear reduction in the horizontal fluid velocity at the baffle, where the fluid motion is restricted as it passes through it. In panels (c,d) the baffle porosity is larger, and the difference in the fluid heights at the baffle is reduced, while in panels (e,f) the baffle is even more porous and the difference in the fluid levels in each region is reduced further. In fact, in this case the free-surface elevations are almost continuous across the baffle. The horizontal velocity value at the baffle is also much less reduced in this final case, meaning the speed of the fluid is altered less by the presence of the baffle, and hence the lower decay rate of the coupled system.

In figure 8 we make a comparison of plots of $h(x,t)$ and $u(x,t)$ for $\gamma = 0.8(1 + 0.2i)$ (solid lines) and $\gamma = 0.8$ (dashed lines). Here we have increased the size of γ_i compared to the real part to 20%, in order to exaggerate the changes to $h(x,t)$ and $u(x,t)$, but as we saw in figure 5, the effect on the lowest frequency mode when $s_i \neq 0$ is small. In fact, it is hard to make any meaningful observation in figure 8, because as γ changes, both s_r and s_i change, hence the results in this figure include a small phase change as well as a change in decay rate. Discerning the difference between these two features is difficult in this figure.

Thus far we have fixed the non-dimensional parameters R and G, but in figure 9 we examine how the decay rate of the system, s_i, varies for different (G, R) combinations for $\gamma \in \mathbb{R}$. The results show that the maximum decay rate always occurs for $\mu = 0.5$ (i.e. for equally sized regions), with the value of $\gamma \in [0, 1.5]$, i.e. close to the rigid baffle limit. For $(G, R) = (7, 0.5)$ in panel (b) the rate of damping is significantly increased, which is due to the spring being stiff in this case but with a heavy fluid mass in the vessel. In this case the horizontal velocities in the fluid are larger than in (a) (weak spring, heavy fluid), and hence the fluid is slowed more dramatically by the baffle. In panel (c) we have a light fluid (heavy vessel) and a weak spring, hence damping rates are low (due to low fluid velocities in the system). Also, the largest decay rates for this configuration are concentrated in a narrow band of small porosity values. While in panel (d) where we have a light fluid and a strong spring, we have a much larger region of the (γ, μ)-plane where the decay rate of this mode is $\geq \frac{1}{4} s_i^{\max}$. Hence in a physical system with these parameters there is a
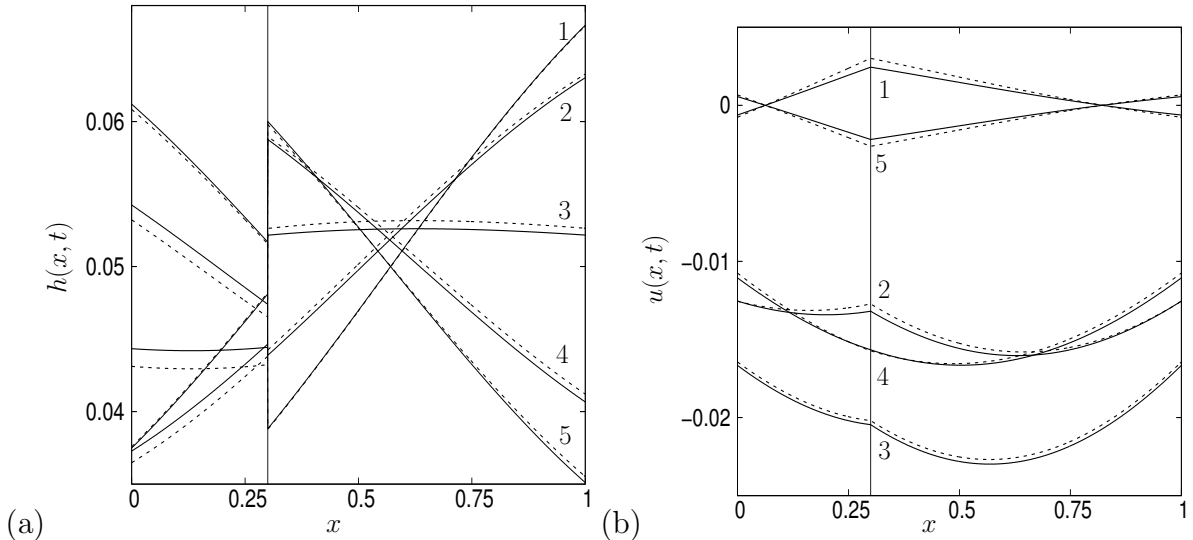
Figure 8: Plot of the non-dimensional free-surface elevation $h_j(x,t)$ and horizontal velocity component $u_j(x,t) = \phi_x(x,t)$ for $j = 1,2$ in the shallow-water limit for $(G, R, \delta, \mu, \epsilon) = (1, 0.5, 0.05, 0.3, 0.01)$ at times $t/(2s_r) = 0, \frac{\pi}{4}, \frac{\pi}{2}, \frac{3\pi}{4}, \pi$ numbered 1-5 respectively. The solid lines are the results for the complex value of $\gamma = 0.8(1 + 0.2\mathrm{i})$, while the dashed lines are the corresponding result with $\gamma = 0.8$, as given in figure 7(a,b).

larger margin for error in the construction of the baffle to have a porosity value needed to achieve a quick decay of the system. This could be useful if a rapid decay of any forced oscillations is required, and the porosity of the wall is not able to be altered via some mechanical means.

3.2 Multiple Baffle System

Thus far we have focused on the single baffle problem, but the theory presented in §2 can easily be extended to multiple baffles, potentially each with a different porosity value. In the final part of this paper we consider the case of multiple, identical baffles, which are equally spaced in the vessel. Hence we only introduce one further parameter, M, which is the number of baffles. The case $M = 1$ we have extensively covered.

The challenge in this case is, despite the simple characteristic equation for the $M = 1$ case in (2.48), this expression very easily becomes complex and unwieldy as M increases. Hence we consider two simplifications, we only consider the limit of shallow-water fluids, and we consider direct numerical solutions to the governing boundary condition equations, rather than forming the characteristic equation analytically and then solving this numerically. To this end, we can write the non-dimensional shallow-water velocity potential in each vessel region from (2.25) as

$$\phi_j(x) = \widehat{A}_j(x) = \widehat{B}_j \cos(2s(x - x_{j-1})) + \widehat{C}_j \sin(2s(x - x_{j-1})),$$

where

$$x_j = \frac{j}{M+1} \quad \text{for} \quad j = 0, ..., M+1,$$

are the dimensionless positions of the vessel side walls and baffles. Here there is no longer a dependence on y as we are in the shallow-water limit, and the hats denote these constants
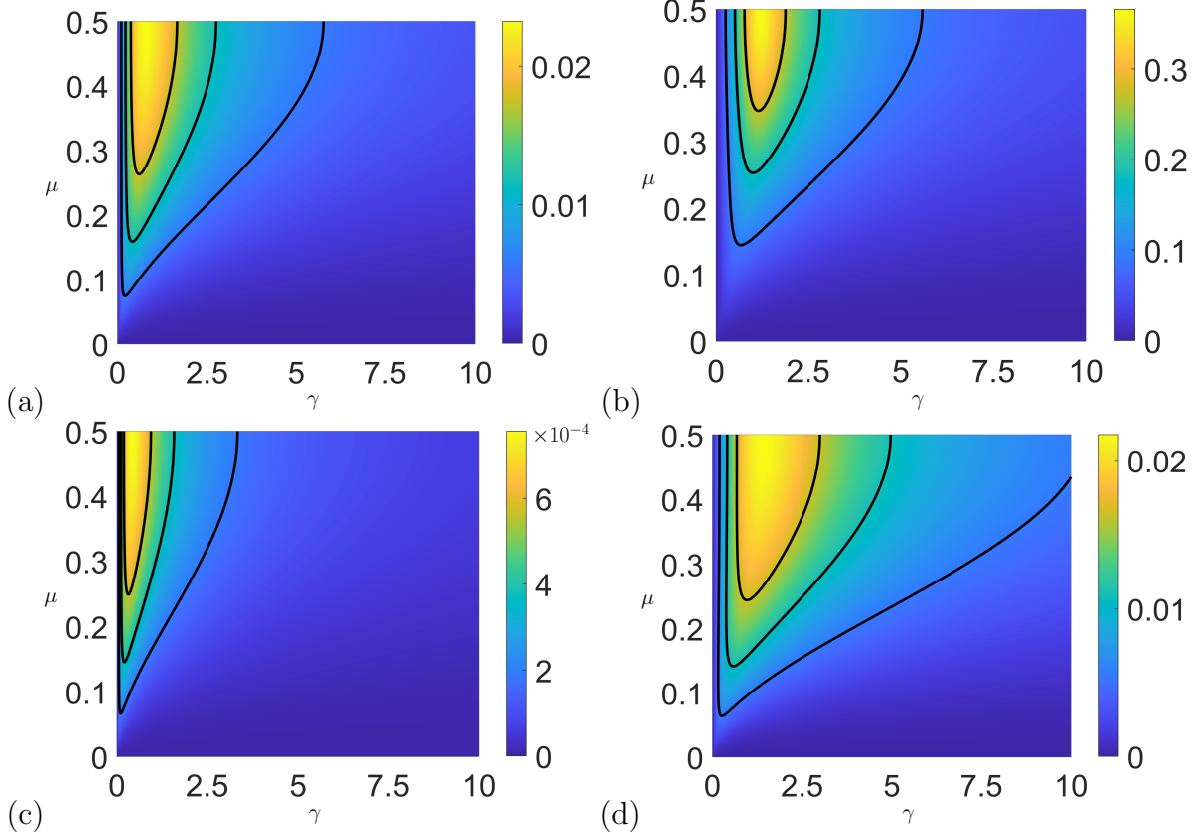
Figure 9: Plots of the decay rate $s_i(\gamma, \mu)$ for (a) $(R, G) = (0.5, 1)$, (b) $(R, G) = (0.5, 7)$, (c) $(R, G) = (5, 1)$ and (d) $(R, G) = (5, 7)$. The black contours signify the values $\frac{1}{4}s_i^{\max}$, $\frac{1}{2}s_i^{\max}$ and $\frac{3}{4}s_i^{\max}$ in each case.

are dimensionless. This solution satisfies all required equations except for the side-wall, and baffle boundary conditions, which fix the constants $\widehat{B}_j$ and $\widehat{C}_j$. For the M baffle problem the boundary conditions to be satisfied are

$$
\begin{aligned}
\widehat{A}_{1x}(x_0) &= \mathrm{i}sQ, \\
\widehat{A}_{1x}(x_1) = \widehat{A}_{2x}(x_1) &= \mathrm{i}sQ + \mathrm{i}\gamma s(\widehat{A}_2(x_1) - \widehat{A}_1(x_1)), \\
\widehat{A}_{2x}(x_2) = \widehat{A}_{3x}(x_2) &= \mathrm{i}sQ + \mathrm{i}\gamma s(\widehat{A}_3(x_2) - \widehat{A}_2(x_2)), \\
\vdots &= \vdots \\
\widehat{A}_{(M+1)x}(x_{M+1}) &= \mathrm{i}sQ,
\end{aligned}
$$

which leads to $2M+2$ equations for the $2M+3$ unknowns ($\widehat{B}_j$, $\widehat{C}_j$ and Q). These equations together with the vessel equation (2.24), which in this notation becomes

$$
\mathrm{i}s \sum_{j=1}^{M+1} \left[\widehat{A}_j(x_j) - \widehat{A}_j(x_{j-1}) \right] + \left[G - Rs^2 \right] Q = 0,
$$

can be written as the $2M+3$ matrix system $\mathbf{B}\mathbf{z} = \mathbf{0}$ where $\mathbf{z} = (\widehat{B}_1, \widehat{C}_1, ..., \widehat{B}_{M+1}, \widehat{C}_{M+1}, Q)^T$.

The characteristic equation would then be found from solving $\det(\mathbf{B})(s) = 0$, such that there is a non-trivial solution to the above system. Here, rather than formulate this
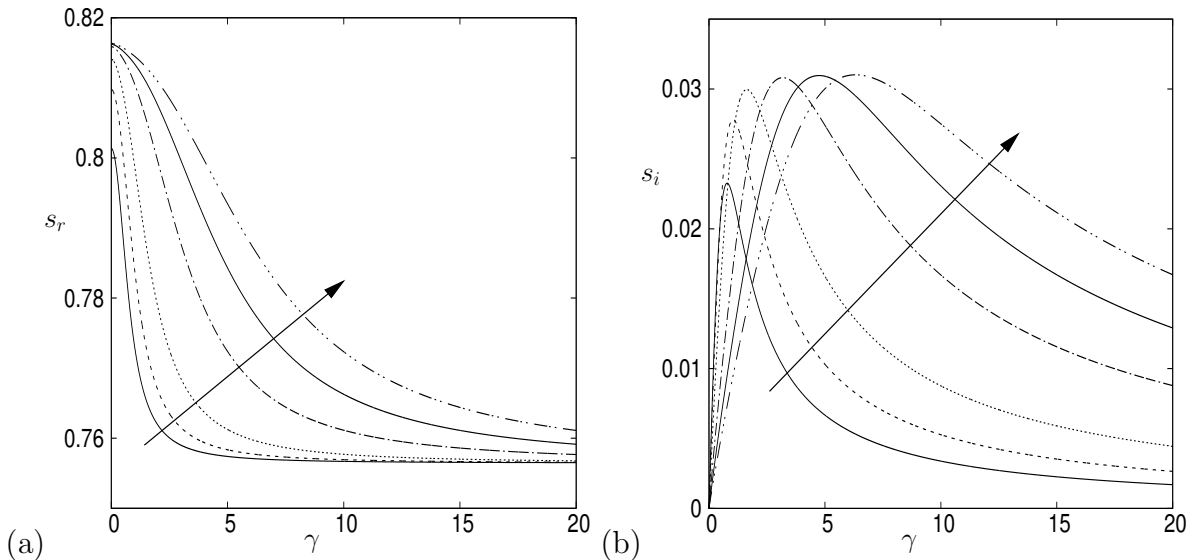
Figure 10: Plot of (a) $s_r(\gamma)$ and (b) $s_i(\gamma)$ in the shallow-water limit with $(G, R) = (1, 0.5)$, for multiple, equally spaced porous baffles. The arrows indicate an increase in the value of M with $M = 1, 2, 4, 9, 14$ and 19 presented.

determinant analytically, we calculate s directly via Newton iterations, using the Jacobi formula to determine the derivative of the determinant with respect to s.

In figure 10 we consider results for $s = s_r + \mathrm{i}s_i$ for $(G, R) = (1, 0.5)$ and values of $M = 1, 2, 4, 9, 14$ and 19 with $\gamma \in \mathbb{R}$. The case $M = 1$ corresponds to the $\mu = 0.5$ case presented in figure 6 and shows a peak decay rate of the system located close to $\gamma = 0$. As the number of baffles is increased what we find is that the maximum decay rate, $s_i^{\max}$, increases to a maximum value at $s_i^{\max} \approx 0.031$ for $M = 19$, which is similar to the maximum decay rate when $M = 9$, i.e. the increase in decay rate slows for large M. The reason for this slow down in increasing $s_i^{\max}$ is due to what can be seen in panel (a), where as M increases, the maximum frequency of the multi-baffled vessel at $\gamma = 0$ changes only by a small amount, hence the difference $s_r(\infty) - s_r(0)$ becomes almost constant, which in turn drives the maximum value of s_i. The significant conclusion of the result in figure 10 is that placing more equally spaced, porous baffles into a system initially increases the decay rate, but only up to about $M = 9$ baffles in this example, after which the increased decay rate return is minimal. However, what is notable is that the range of γ values over which there is significant decay is greatly increased. This means that rapid decay can be achieved in a system with baffles with larger γ (which might be easier and cheaper to manufacture) rather than having to acquire baffles with small γ, which might be more expensive to manufacture.

4   Conclusions

In this paper we studied the coupled vessel plus contained fluid, motion for rectilinear vessel motions and two-dimensional fluid motions, in the presence of porous, surface piercing baffles. The fluid was assumed to be inviscid, incompressible and irrotational, such that it can be written in terms of a velocity potential in each connected region. By linking each region together via a porous wall transmission condition given by Darcy's

law, and seeking normal mode solutions about a quiescent state, we derived an explicit characteristic equation in the single baffle case. The characteristic equation correctly reduced to the two compartment impermeable baffle case of [7] and the single compartment case of [35] in the limits $|\gamma| \to 0$ and $|\gamma| \to \infty$ respectively, where γ is the non-dimensional baffle porosity parameter.

The presented results for both finite-depth and shallow-water fluids showed that the modes which couple to the vessel motion (i.e. not symmetric free-modes in a stationary vessel) decay exponentially in time, i.e. they have a complex non-dimensional frequency $s = s_r + \mathrm{i} s_i$ with $s_i \geq 0$. There was no obvious connection between the mode's decay rate, s_i, and its frequency, s_r, but the maximum decay rate for each mode occurred in a region of γ values where s_r sharply varied from its $|\gamma| = 0$ value to its $|\gamma| = \infty$ value. The lowest frequency mode typically had the smallest maximum decay rate (except in the special vessel configurations with neutral modes), and hence this mode is expected to be most significant in real systems which contain a superposition of these modes, at moderate times.

For a vessel configuration with M equally spaced identical baffles we were able to show that the maximum decay rate for the lowest frequency mode increased as M was increased towards some limiting value for large M. It was also found that the range of baffle porosity values γ over which the decay rate was, say, $\geq \frac{3}{4} s_i^{\max}$ increased with M. This means that in a physical system in order to achieve rapid damping, a large number of baffles should be installed. This could however, be expensive, and so a smaller number of baffles could be used if the wall porosity is tuned such that the mode frequency generated by some external mechanism lies close to a value where the lowest frequency mode decays fastest.

Future work of potential interest is to incorporate baffles which have a time dependent porosity, such as a wall with movable slats. If the time-scale of the wall porosity change is faster than the period of the fluid oscillations, then modes could be manipulated to some maximal decay rate, meaning any induced oscillations could be quickly removed. This could be particularly significant in Tuned Liquid Dampers in highrise buildings [45]. This is considered in future work.

Acknowledgements

A Free Sloshing Modes

In this appendix we examine the form of the eigenvector $(B_{10}, B_{20}, \widehat{q})^T$ of (2.41) for the case when $\det(\widehat{\mathbf{A}}) = 0$ for $\widehat{\mathbf{A}}$ in (2.38). We show that these modes are either trivial solutions to the system or free-sloshing modes in a stationary vessel, $\widehat{q} \equiv 0$. We now consider two distinct cases.

A.1   Case 1: $\sin k_0 L_1 = \sin k_0 L_2 = 0$

One solution of $\det(\widehat{\mathbf{A}}) = 0$ is when both $\sin k_0 L_2 = 0$ and $\sin k_0 L_1 = 0$ simultaneously. As noted in the main text, this amounts to the compartment lengths being related by $m L_2 = m' L_1$ for $m, m' \in \mathbb{N}$. In this case the governing equations of (2.41) reduce to

$$
\begin{aligned}
-\mathrm{i}\omega c_0(\cos k_0 L_1 - \cos k_0 L_2)\widehat{q} &= 0, \\
\mathrm{i}\omega\beta(-\cos k_0 L_1 B_{10} + \cos k_0 L_2 B_{20}) &= \mathrm{i}\omega c_0(\cos k_0 L_1 - 1)\widehat{q}, \\
\mathrm{i}\omega\rho H c_0(\cos k_0 L_1 - 1)B_{10} - \mathrm{i}\omega\rho H c_0(1 - \cos k_0 L_1)B_{20} + \Theta\widehat{q} &= 0,
\end{aligned}
$$

with Θ given in (2.40). We now consider three separate sub-cases of this case.

A.1.1   Sub-case A: $\cos k_0 L_1 = \cos k_0 L_2 = 1$

Here both m and m' are even, and under these conditions the three equations above reduce to

$$
B_{10} = B_{20}, \quad \text{and} \quad \widehat{q} = 0.
$$

Hence, this results in free-sloshing in a stationary vessel with symmetric free-surface profiles in each region, as shown for an example in figure 11(a).

A.1.2   Sub-case B: $\cos k_0 L_1 = \cos k_0 L_2 = -1$

Here both m and m' are odd and under these conditions the three equations above reduce to

$$
\beta(B_{10} - B_{20}) = -2c_0\widehat{q}, \quad \text{and} \quad 2\mathrm{i}\omega\rho H c_0(-B_{10} + B_{20}) + \Theta\widehat{q} = 0.
$$

These equations can be combined together into

$$
\left[\frac{4\mathrm{i}\omega\rho H c_0^2}{\beta} + \Theta\right]\widehat{q} = 0.
$$

The bracketed quantity is not zero for all parameter values, hence again $\widehat{q} = 0$ and $B_{10} = B_{20}$ is arbitrary. These are again free-sloshing modes in a stationary vessel, but this time the modes are anti-symmetric in each region. Hence each region generates an equal and opposite force on the vessel walls during its motion, which keeps the vessel stationary. An example of these anti-symmetric modes are plotted in figure 11(b).

A.1.3   Sub-case $\cos k_0 L_1 = 1$ and $\cos k_0 L_2 = -1$ (or vice versa)

In this case either m or m' is even, while the other is odd, and under these conditions the three equations above reduce to

$$
\begin{aligned}
-2\mathrm{i}\omega c_0\widehat{q} &= 0, \\
-\mathrm{i}\omega\beta(B_{10} + B_{20}) &= 0, \\
2\mathrm{i}\omega\rho H c_0 B_{20} + \Theta\widehat{q} &= 0.
\end{aligned}
$$

Thus $\widehat{q} = 0$ from the first equation, and so the third equation gives $B_{20} = 0$, and finally $B_{10} = 0$ from the second equation. Hence the result is the trivial case. This is consistent with the previous results, because in this case the mode in one region is symmetric, i.e. produces no lateral force on the vessel, while in the second region the free-surface is ant-symmetric and is producing a lateral force on the vessel. Hence this scenario cannot occur. An example of this case is plotted in figure 11(c).
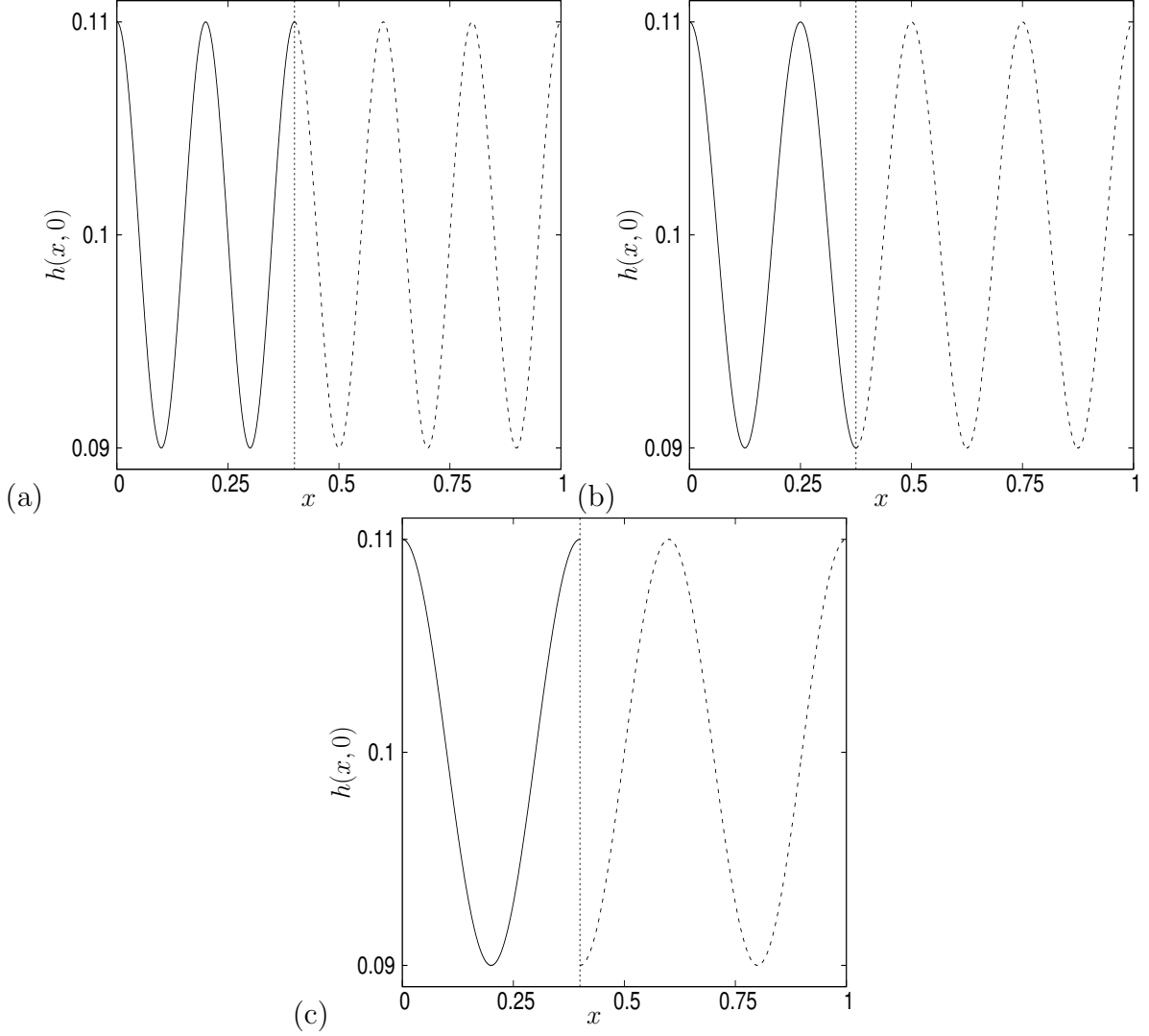
Figure 11: Plot of the free-surface elevation $h(x, 0)$ for the three sub-cases (a) sub-case A with $(L_1, L_2) = (0.4, 0.6)$, (b) sub-case B with $(L_1, L_2) = (0.375, 0.625)$ and (c) sub-case C with $(L_1, L_2) = (0.4, 0.6)$. In each case $H = 0.1$ and $\epsilon = 0.01$ and the vertical dotted line represents the baffle. Here each mode is a neutral mode with $s \in \mathbb{R}$, i.e. a zero decay rate. The fluid frequencies in each section are the same, such that the fluid waves meet at the baffle so no fluid passes through the baffle. Hence the fluid heights are continuous across the baffle in (a) and (b).

A.2 Case 2: $\omega = -\dfrac{\mathrm{i}k_0}{\beta(\cot k_0 L_1 + \cot k_0 L_2)}$

In this case we introduce the new constants

$$D_{j0} = \frac{B_{j0}}{\cot k_0 L_1 + \cot k_0 L_2}, \quad P = \frac{\widehat{q}}{(\cot k_0 L_1 + \cot k_0 L_2)^2},$$

and then the governing equations can be written as

$$k_0 \sin k_0 L_1 D_{10} + k_0 \sin k_0 L_2 D_{20} = -\frac{k_0 c_0}{\beta}(\cos k_0 L_2 - \cos k_0 L_1)P,$$

$$k_0 \sin k_0 L_1 D_{10} + k_0 \sin k_0 L_2 D_{20} = \frac{k_0 c_0 \sin k_0 L_2}{\beta \sin k_0 L_1}\left[(\cos k_0 L_1 - 1)(\cot k_0 L_1 + \cot k_0 L_2)\right.$$
$$\left. + \sin k_0 L_1 + \sin k_0 L_2\right]P,$$

$$k_0 \rho H c_0 \left[(\cos k_0 L_1 - 1)D_{10} + (1 - \cos k_0 L_2)D_{20}\right] + (\cot k_0 L_1 + \cot k_0 L_2)^2 \Theta P = 0.$$

Eliminating the D_{j0} constants from the first 2 equations leads to

$$\left[\frac{\sin k_0 L_2}{\sin k_0 L_1}\left[(\cos k_0 L_1 - 1)(\cot k_0 L_1 + \cot k_0 L_2) + \sin k_0 L_1 + \sin k_0 L_2\right]\right.$$

$$\left. + \cos k_0 L_2 - \cos k_0 L_1\right]P = 0,$$

which implies that $P = 0$, as the square bracket is not zero for all parameter values. The resulting equations then lead to $D_{10} = D_{20} = 0$, i.e. the trivial solution for this value of ω.

B Asymptotic Solutions for the Non-Dimensional Frequency, s

In this appendix we calculate the asymptotic form of the non-dimensional frequency s for the case $\gamma \in \mathbb{R}$ in the limits $\gamma \ll 1$ and $\gamma \gg 1$.

B.1 Asymptotic Frequencies in $\gamma \ll 1$ Limit

We can identify the form of the complex sloshing frequency s in the limit as $\gamma \to 0$ by forming an asymptotic expansion of all variables which depend on s, in the form

$$
\begin{aligned}
s &= s_0 + \gamma s_1 + O(\gamma^2), \\
\alpha_0 &= \alpha_{00} + \gamma \alpha_{01} + O(\gamma^2), \\
\alpha_n &= \alpha_{n0} + \gamma \alpha_{n1} + O(\gamma^2), \\
c_0^2 &= c_{00}^2 + \gamma c_{01}^2 + O(\gamma^2), \\
c_n^2 &= c_{n0}^2 + \gamma c_{n1}^2 + O(\gamma^2), \\
\Theta_0 &= \Theta_{00} + \gamma \Theta_{01} + O(\gamma^2), \\
\Theta_1 &= \Theta_{10} + \gamma \Theta_{11} + O(\gamma^2), \\
\Theta_2 &= \Theta_{20} + \gamma \Theta_{21} + O(\gamma^2).
\end{aligned}
\tag{2.51}
$$

The process documented below could be extended to achieve higher order accuracy by computing more terms in the asymptotic series for s. However, for the purposes of this paper there are no clear benefits to computing past the first two terms, and hence we stop our expansions at this point.

By considering the eigenvalue problems for α_0 and α_n in (2.45), we can deduce expressions which link α_{00} to s_0 and α_{01} to s_1 etc. Inserting the expansions (2.51) into the first equation of (2.45) gives

$$
\begin{aligned}
O(1): &\quad \alpha_{00} \tanh \alpha_{00}\delta - 4\delta s_0^2 = 0, \\
O(\gamma): &\quad \alpha_{01} \tanh \alpha_{00}\delta + \alpha_{00}\alpha_{01} \operatorname{sech}^2 \alpha_{00}\delta - 8\delta s_0 s_1 = 0.
\end{aligned}
\tag{2.52}
$$

Hence at leading order this is just the usual eigenvalue problem which needs to be solved given an s_0 value, while the second equation shows that α_{01} and s_1 are linked via the linear expression,

$$
\alpha_{01} = \frac{8\delta\alpha_{00}s_0}{(\alpha_{00}^2 + 4\delta s_0^2 - 16\delta^2 s_0^4)} s_1.
$$

Similarly for the evanescent modes, the second equation of (2.45) becomes

$$
\begin{aligned}
O(1): &\quad \alpha_{n0} \tan \alpha_{n0}\delta + 4\delta s_0^2 = 0, \\
O(\gamma): &\quad \alpha_{n1} \tan \alpha_{n0}\delta + \alpha_{n0}\alpha_{n1} \sec^2 \alpha_{00}\delta + 8\delta s_0 s_1 = 0,
\end{aligned}
\tag{2.53}
$$

and so at $O(\gamma)$

$$
\alpha_{n1} = -\frac{8\delta\alpha_{n0}s_0}{(\alpha_{n0}^2 - 4\delta s_0^2 + 16\delta^2 s_0^4)} s_1.
$$

By the same process the coefficients in (2.32) gives

$$
\begin{aligned}
O(1): &\quad c_{00}^2 = \frac{4\sinh^2(\alpha_{00}\delta)}{\alpha_{00}\delta(2\alpha_{00}\delta + \sinh 2\alpha_{00}\delta)}, \\
O(\gamma): &\quad c_{01}^2 = -\frac{c_{00}^2\alpha_{01}}{\alpha_{00}} \left(1 - 2\delta\alpha_{00} \coth \alpha_{00}\delta + \delta^2\alpha_{00}^2 c_{00}^2 \coth^2 \alpha_{00}\delta\right), \\
O(1): &\quad c_{n0}^2 = \frac{4\sin^2 \alpha_{n0}\delta}{\alpha_{n0}\delta(2\alpha_{n0}\delta + \sin 2\alpha_{n0}\delta)}, \\
O(\gamma): &\quad c_{n1}^2 = -\frac{c_{n0}^2\alpha_{n1}}{\alpha_{n0}} \left(1 - 2\delta\alpha_{n0} \cot \alpha_{n0}\delta + \delta^2\alpha_{n0}^2 c_{n0}^2 \cot^2 \alpha_{n0}\delta\right).
\end{aligned}
\tag{2.54}
$$

Therefore, substituting these expansions into the characteristic equation gives,

$$
\alpha_{00} \sin \alpha_{00}\mu \sin \alpha_{00}(1-\mu) \left[2s_0^2 c_{00}^2 \left(\tan \frac{1}{2}\alpha_{00}\mu + \tan \frac{1}{2}\alpha_{00}(1-\mu)\right) - \alpha_{00}\Theta_{00}\right] = 0.
$$

This characteristic equation is exactly that given in [7] for the case of two separate compartments with equal mean fluid depths. Solving this characteristic equation gives the leading order value of the frequency s_0 which is purely real. The next order correction

term comes from the $O(\gamma)$ part of the characteristic equation which states,

$$4\alpha_{00}s_0c_{00}^2\sin\alpha_{00}\mu\sin\alpha_{00}(1-\mu)\left(\tan\frac{1}{2}\alpha_{00}\mu+\tan\frac{1}{2}\alpha_{00}(1-\mu)\right)s_1$$

$$+\left[2\alpha_{00}s_0^2\sin\alpha_{00}\mu\sin\alpha_{00}(1-\mu)\left(\frac{\mu}{2}\sec^2\frac{1}{2}\alpha_{00}\mu+\frac{(1-\mu)}{2}\sec^2\frac{1}{2}\alpha_{00}(1-\mu)\right)\right.$$

$$+2\left(\alpha_{00}s_0^2(1-\mu)\sin\alpha_{00}\mu\cos\alpha_{00}(1-\mu)\right.$$

$$+(\alpha_{00}s_0^2\mu\cos\alpha_{00}\mu+s_0^2\sin\alpha_{00}\mu)\sin\alpha_{00}(1-\mu))\left(\tan\frac{1}{2}\alpha_{00}\mu+\tan\frac{1}{2}\alpha_{00}(1-\mu)\right)\Big]c_{00}^2\alpha_{01}$$

$$-(\alpha_{00}^2(1-\mu)\sin\alpha_{00}\mu\cos\alpha_{00}(1-\mu)+(\alpha_{00}^2\mu\cos\alpha_{00}\mu+2\alpha_{00}\sin\alpha_{00}\mu)\sin\alpha_{00}(1-\mu))\Theta_{00}\alpha_{01}$$

$$+2\alpha_{00}s_0^2c_{01}^2\sin\alpha_{00}\mu\sin\alpha_{00}(1-\mu)\left(\tan\frac{1}{2}\alpha_{00}\mu+\tan\frac{1}{2}\alpha_{00}(1-\mu)\right)$$

$$-2\mathrm{i}s_0^3c_{00}^2(1-\cos\alpha_{00})+\mathrm{i}\alpha_{00}s_0\Theta_{00}\sin\alpha_{00}-(\Theta_{01}-\mathrm{i}\Theta_{20})\alpha_{00}^2\sin\alpha_{00}\mu\sin\alpha_{00}(1-\mu)=0,$$

where

$$\Theta_{00} = G-Rs_0^2-2s_0^2\sum_{n=1}^{\infty}\frac{c_{n0}^2}{\alpha_{n0}}\left(\tanh\frac{1}{2}\alpha_{n0}\mu+\tanh\frac{1}{2}\alpha_{n0}(1-\mu)\right),$$

$$\Theta_{01} = -2Rs_0s_1$$
$$-\sum_{n=1}^{\infty}\left[\frac{2}{\alpha_{n0}^2}\left(s_0^2\alpha_{n0}c_{n1}^2+2s_0s_1\alpha_{n0}c_{n0}^2-s_0^2c_{n0}^2\alpha_{n0}\right)\left(\tanh\frac{1}{2}\alpha_{n0}\mu+\tanh\frac{1}{2}\alpha_{n0}(1-\mu)\right)\right.$$
$$+\frac{2s_0^2c_{n0}^2\alpha_{n1}}{\alpha_{n0}}\left(\frac{\mu}{2}\operatorname{sech}^2\frac{1}{2}\alpha_{n0}\mu+\frac{(1-\mu)}{2}\operatorname{sech}^2\frac{1}{2}\alpha_{n0}(1-\mu)\right)\bigg],$$

$$\Theta_{20} = -s_0^3\sum_{n=1}^{\infty}\frac{c_{n0}^2}{\alpha_{n0}}\left(\tanh\frac{1}{2}\alpha_{n0}\mu+\tanh\frac{1}{2}\alpha_{n0}(1-\mu)\right)^2.$$

This equation is solved to give s_1, using (2.52)-(2.54) to eliminate these variables in favour of s_1. The value for s_1 is purely imaginary. Results of this approximation are given in figure 4.

B.2   Asymptotic Frequencies in $\gamma \gg 1$ Limit

The mechanism for calculating the asymptotic frequencies for $\gamma \gg 1$ follows a similar calculation as for $\gamma \ll 1$ in §B.1. The difference being that we introduce the small parameter $\nu = \gamma^{-1}$ and expand as before. Therefore, this time we write

$$\begin{aligned}
s &= s_0+\nu s_1+O(\nu^2),\\
\alpha_0 &= \alpha_{00}+\nu\alpha_{01}+O(\nu^2),\\
\alpha_n &= \alpha_{n0}+\nu\alpha_{n1}+O(\nu^2),\\
c_0^2 &= c_{00}^2+\nu c_{01}^2+O(\nu^2),\\
c_n^2 &= c_{n0}^2+\nu c_{n1}^2+O(\nu^2),
\end{aligned}$$

and the values of $\alpha_{00},\alpha_{01},\alpha_{n0}$ and α_{n1}, along with $c_{00}^2,c_{01}^2,c_{n0}^2$ and c_{n1}^2, are again linked to s_0 and s_1 via equations (2.52)-(2.54). The significant difference in this derivation of the

asymptotic frequencies, is here we find that

$$\begin{aligned}
\Theta_0 &= \widetilde{\Theta}_{00} + \nu\widetilde{\Theta}_{01} + O(\nu^2), \\
\Theta_1 &= \nu^2\widetilde{\Theta}_{10} + \nu^3\widetilde{\Theta}_{11} + O(\nu^4), \\
\Theta_2 &= \nu^2\widetilde{\Theta}_{20} + O(\nu^3).
\end{aligned}$$

Thus the leading order characteristic equation is

$$s_0 \sin\alpha_{00}\left[\alpha_{00}(\widetilde{\Theta}_{00} + \widetilde{\Theta}_{10}) - 2s_0^2c_{00}^2\tan\alpha_{00}\right] = 0,$$

which is simply the one compartment form of the characteristic equation given by [35] and again is purely real. At $O(\nu)$ the correction term s_1, which again is purely imaginary, is found by solving

$$\begin{aligned}
&\left[-6is_0^2c_{00}^2(1-\cos\alpha_{00}) + i\alpha_{00}\sin\alpha_{00}(\widetilde{\Theta}_{00} + \widetilde{\Theta}_{10})\right]s_1 \\
&+ \left[-2is_0^3c_{00}^2\sin\alpha_{00} + is_0(\sin\alpha_{00} + \alpha_{00}\cos\alpha_{00})(\widetilde{\Theta}_{00} + \widetilde{\Theta}_{10})\right]\alpha_{01} \\
&+ 2\alpha_{00}s_0^2c_{00}^2\sin\alpha_{00}\mu\sin\alpha_{00}(1-\mu)\left(\tan\frac{1}{2}\alpha_{00}\mu + \tan\frac{1}{2}\alpha_{00}(1-\mu)\right) - 2is_0^3c_{01}^2(1-\cos\alpha_{00}) \\
&- \alpha_{00}^2\sin\alpha_{00}\mu\sin\alpha_{00}(1-\mu)(\widetilde{\Theta}_{00} + \widetilde{\Theta}_{10}) + is_0\alpha_{00}\sin\alpha_{00}(\widetilde{\Theta}_{01} + \widetilde{\Theta}_{11} - i\widetilde{\Theta}_{20}) = 0,
\end{aligned}$$

where

$$\begin{aligned}
\widetilde{\Theta}_{00} &= G - Rs_0^2, \\
\widetilde{\Theta}_{01} &= -2Rs_0s_1, \\
\widetilde{\Theta}_{20} &= -s_0\sum_{n=1}^{\infty}c_{n0}^2\alpha_{n0}\frac{\left(\tanh\frac{1}{2}\alpha_{n0}\mu + \tanh\frac{1}{2}\alpha_{n0}(1-\mu)\right)^2}{\left(\coth\alpha_{n0}\mu + \coth\alpha_{n0}(1-\mu)\right)^2}, \\
\widetilde{\Theta}_{10} &= -2s_0^2\sum_{n=1}^{\infty}\frac{c_{n0}^2}{\alpha_{n0}}\tanh\frac{1}{2}\alpha_{n0}, \\
\widetilde{\Theta}_{11} &= -\sum_{n=1}^{\infty}\left[\frac{2s_0}{\alpha_{n0}^2}(s_0c_{n1}^2\alpha_{n0} + 2s_1c_{n0}^2\alpha_{n0} - s_0c_{n0}^2\alpha_{n1})\tanh\frac{1}{2}\alpha_{n0} + \frac{s_0^2c_{n0}^2\alpha_{n1}}{\alpha_{n0}}\operatorname{sech}^2\frac{1}{2}\alpha_{n1}\right].
\end{aligned}$$

Results of this approximation are given in figure 4.

References

[1] H. C. Mayer and R. Krechetnikov. Walking with coffee: why does it spill? *Phys. Rev. E*, 85:046117, 2012.

[2] B. H. Adee and I. Caglayan. The effects of free water on deck on the motions and stability of vessels. In *Proc. Second Inter. Conf. Stab. Ships and Ocean Vehicles*, Tokyo, October 1982. SNAME, Springer (Berlin).

[3] H. Ockendon and J. R. Ockendon. How to mitigate sloshing. *SIAM Review*, 59(4):905–911, 2017.

[4] H. N. Abramson. *The Dynamic Behavior of Liquids in Moving Containers.* NASA SP-106 (Washington D. C.), 1966.

[5] R. A. Ibrahim. *Liquid Sloshing Dynamics.* Cambridge University Press (Cambridge), 2005.

[6] G. W. Housner, L. A. Bergman, T. K. Caughey, Anastassios G. Chassiakos, R. O. Claus, S. F. Masri, R. E. Skelton, T. T. Soong, B. F. Spencer, and J. T. P. Yao. Structural Control: Past, Present, and future. *J. Eng. Mech.*, 123(9):897–971, 1997.

[7] M. R. Turner, T. J. Bridges, and H. Alemi Ardakani. Dynamic coupling in Cooker's sloshing experiment with baffles. *Phys. Fluids*, 25(11):112102, 2013.

[8] H. Alemi Ardakani and M. R. Turner. Numerical simulations of dynamic coupling between shallow-water sloshing and horizontal vessel motion with baffles. *Fluid Dyn. Res.*, 48(3):035504, 2016.

[9] M. J. Tait, A. A. El Damatty, N. Isyumov, and M. R. Siddique. Numerical flow models to simulate tuned liquid dampers (TLD) with slat screens. *J. Fluids and Struct.*, 20(8):1007–1023, 2005.

[10] M. Maravani and M. S. Hamed. Numerical modeling of sloshing motion in a tuned liquid damper outfitted with a submerged slat screen. *Int. J. Numer. Methods Fluids*, 65(7):834–855, 2011.

[11] M. Isaacson and S. Premasiri. Hydrodynamic damping due to baffles in a rectangular tank. *Can. J. Civ. Eng.*, 28(4):608–616, 2001.

[12] L. Yu, M. Xue, and J. Zheng. Experimental study of vertical slat screens effects on reducing shallow water sloshing in a tank under horizontal excitation with a wide frequency range. *Ocean Eng.*, 173:131–141, 2019.

[13] S. K. Poguluri and I. H. Cho. Liquid sloshing in a rectangular tank with vertical slotted porous screen: Based on analytical, numerical, and experimental approach. *Ocean Eng.*, 189:106373, 2019.

[14] T. Nasar and S. A. Sannasiraj. Sloshing dynamics and performance of porous baffle arrangements in a barge carrying liquid tank. *Ocean Eng.*, 183:24–39, 2019.

[15] Q. Zang, H. Fang, J. Liu, and G. Lin. Boundary element model for investigation of the effects of various porous baffles on liquid sloshing in the two dimensional rectangular tank. *Eng. Anal. Bound. Elem.*, 108:484–500, 2019.

[16] A. George and I. H. Cho. Anti-sloshing effects of a vertical porous baffle in a rolling rectangular tank. *Ocean Eng.*, 214:107871, 2020.

[17] L. Yu, M. Xue, and A. Zhu. Numerical investigation of sloshing in rectangular tank with permeable baffle. *J. Mar. Sci. Eng.*, 8(9):671, 2020.

[18] J. Wu, W. Zhong, J. Fu, T. N. Ng, L. Sun, and P. Huang. Investigation on the damping of rectangular water tank with bottom-mounted vertical baffles: Hydrodynamic interaction and frequency reduction effect. *Engineering Structures*, 245:112815, 2021.

[19] H. Saghi, T. Mikkola, and S. Hirdaris. The influence of obliquely perforated dual-baffles on sway induced tank sloshing dynamics. *Proceedings of the Institution of Mechanical Engineers, Part M: Journal of Engineering for the Maritime Environment*, 235(4):905–920, 2021.

[20] X. Jin, H. Zheng, M. Liu, F. Zhang, Y. Yang, and L. Ren. Damping effects of dual vertical baffles on coupled surge-pitch sloshing in three-dimensional tanks: A numerical investigation. *Ocean Eng.*, 261:112130, 2022.

[21] M. A. Goudarzi and P. Farshadmanesh. Numerical evaluation of hydrodynamic damping due to the upper mounted baffles in real scale tanks. *Soil Dyn. Earthq. Eng.*, 77:290–298, 2015.

[22] V. S. Sanapala, M. Rajkumar, K. Velusamy, and B. S. V. Patnaik. Numerical simulation of parametric liquid sloshing in a horizontally baffled rectangular container. *J. Fluids Struct.*, 76:229–250, 2018.

[23] E. O. Tuck. Matching problems involving flow through small holes. *Adv. Appl. Mech.*, 15:89–158, 1975.

[24] A. T. Chwang. A porous-wavemaker theory. *J. Fluid Mech.*, 132:395–406, 1983.

[25] X. Yu and A. T. Chwang. Wave motion through porous structures. *J. Eng Mech.*, 120(5):989–1008, 1994.

[26] B. Straughan. *Stability and wave motion in porous media*, volume 165. Springer Science & Business Media, 2008.

[27] H. Behera, S. Mandal, and T. Sahoo. Oblique wave trapping by porous and flexible structures in a two-layer fluid. *Phys. Fluids*, 25(11), 2013.

[28] E. M. Laws and J. L. Livesey. Flow through screens. *Annu. Rev. Fluid Mech.*, 10(1):247–266, 1978.

[29] O. M. Faltinsen, R. Firoozkoohi, and A. N. Timokha. Analytical modeling of liquid sloshing in a two-dimensional rectangular tank with a slat screen. *J. Eng. Math.*, 70:93–109, 2011.

[30] B. Molin. On the added mass and damping of periodic arrays of fully or partially porous disks. *J. Fluid Struct.*, 15(2):275–290, 2001.

[31] O. Kimmoun, B. Molin, and W. Moubayed. Second-order analysis of the interaction of a regular wave train with a vertical perforated wall. *Proceedings of 8èmes Journèes de l'Hydrodynamique*, 5(6):7, 2001.

[32] G. R. Baker, D. I. Meiron, and S. A. Orszag. Generalized vortex methods for free surface flow problems. ii: Radiating waves. *J. Sci. Comput.*, 4(3):237–259, 1989.

[33] A. I. Dyachenko, A. O. Korotkevich, and V. E. Zakharov. Weak turbulent kolmogorov spectrum for surface gravity waves. *Phys. Rev. Lett.*, 92(13):134501, 2004.

[34] J. Wang and D. D. Joseph. Purely irrotational theories of the effect of the viscosity on the decay of free gravity waves. *J. Fluid Mech.*, 559:461–472, 2006.

[35] H. Alemi Ardakani, T. J. Bridges, and M. R. Turner. Resonance in a model for Cooker's sloshing experiment. *Euro. J. Mech. B/Fluids*, 36:25–38, 2012.

[36] P. D. Weidman and M. R. Turner. Experiments on the synchronous sloshing in suspended containers described by shallow-water theory. *J. Fluid Struct.*, 66:331–349, 2016.

[37] I. H. Cho and M. H. Kim. Wave absorbing system using inclined perforated plates. *J. Fluid Mech.*, 608:1–20, 2008.

[38] V. Girault and M. F. Wheeler. Numerical discretization of a Darcy–Forchheimer model. *Numer. Math.*, 110(2):161–198, 2008.

[39] T. Sahoo, M. M. Lee, and A. T. Chwang. Trapping and generation of waves by vertical porous structures. *J. Eng. Mech.*, 126(10):1074–1082, 2000.

[40] H. Behera and C.-O. Ng. Interaction between oblique waves and multiple bottom-standing flexible porous barriers near a rigid wall. *Meccanica*, 53:871–885, 2018.

[41] Y. Li, Y. Liu, and B. Teng. Porous effect parameter of thin permeable plates. *Coast. Eng.*, 48(4):309–336, 2006.

[42] C. M. Linton and P. McIver. *Handbook of Mathematical Techniques for Wave–Structure Interaction.* Chapman & Hall/CRC (Boca Raton), 2001.

[43] M. J. Cooker. Water waves in a suspended container. *Wave Motion*, 20:385–395, 1994.

[44] P. Warnitchai and T. Pinkaew. Modelling of liquid sloshing in rectangular tanks with flow-dampening devices. *Eng, Struct.*, 20(7):593–600, 1998.

[45] A. Kareem, T. Kijewski, and Y. Tamura. Mitigation of motions of tall buildings with specific examples of recent applications. *Wind Struct.*, 2(3):201–251, 1999.